



HAL
open science

SUSD4 controls GLUA2 degradation, synaptic plasticity and motor learning

I. González-Calvo, K. Iyer, M. Carquin, A. Khayachi, F.A. Giuliani, S.M. Sigoillot, J. Vincent, M. Seveno, M. Veleanu, S. Tahraoui, et al.

► **To cite this version:**

I. González-Calvo, K. Iyer, M. Carquin, A. Khayachi, F.A. Giuliani, et al.. SUSD4 controls GLUA2 degradation, synaptic plasticity and motor learning. 2021. hal-03160965v1

HAL Id: hal-03160965

<https://hal.science/hal-03160965v1>

Preprint submitted on 16 Nov 2021 (v1), last revised 5 Mar 2021 (v2)

HAL is a multi-disciplinary open access archive for the deposit and dissemination of scientific research documents, whether they are published or not. The documents may come from teaching and research institutions in France or abroad, or from public or private research centers.

L'archive ouverte pluridisciplinaire **HAL**, est destinée au dépôt et à la diffusion de documents scientifiques de niveau recherche, publiés ou non, émanant des établissements d'enseignement et de recherche français ou étrangers, des laboratoires publics ou privés.

1 **SUSD4 controls GLUA2 degradation, synaptic plasticity and motor learning**

2 **I. González-Calvo^{1,2,8,†}, K. Iyer^{1,†}, M. Carquin¹, A. Khayachi¹, F.A. Giuliani², J. Vincent³,**
3 **M. Séveno⁴, S.M. Sigoillot¹, M. Veleau¹, S. Tahraoui¹, M. Albert¹, O. Vigy⁵, C. Bosso-**
4 **Lefèvre¹, Y. Nadjar⁶, A. Dumoulin⁶, A. Triller⁶, J.-L. Bessereau⁷, L. Rondi-Reig³, P. Isope²,**
5 **F. Selimi^{1*}**

7 **Affiliations:**

8 ¹ Center for Interdisciplinary Research in Biology (CIRB), Collège de France, CNRS, INSERM,
9 PSL Research University, Paris, France.

10 ² Institut de Neurosciences Cellulaires et Intégratives (INCI), CNRS, Université de Strasbourg,
11 Strasbourg, France.

12 ³ Institut Biology Paris Seine (IBPS), Neuroscience Paris Seine (NPS), CeZaMe, CNRS,
13 Sorbonne University, INSERM, Paris, France.

14 ⁴ BioCampus Montpellier, CNRS, INSERM, Université de Montpellier, Montpellier, France.

15 ⁵ Institut de Génomique Fonctionnelle, CNRS, INSERM, Université de Montpellier, Montpellier,
16 France.

17 ⁶ École Normale Supérieure, Institut de Biologie de l'ENS, INSERM, CNRS, PSL Research
18 University, Paris, France.

19 ⁷ Université de Lyon, Université Claude Bernard Lyon 1, CNRS UMR 5310, INSERM U 1217,
20 Institut Neuromyogène, 69008, Lyon, France.

21 ⁸ Present address: Univ. Bordeaux, CNRS, Interdisciplinary Institute for Neuroscience, IINS,
22 UMR 5297, F-33000 Bordeaux, France

23 † Equal contribution.

24 * Correspondence to: fekrije.selimi@college-de-france.fr

25

26

27

28 **Summary**

29 Fine control of protein stoichiometry at synapses underlies brain function and plasticity. How
30 proteostasis is controlled independently for each type of synaptic protein in a synapse-specific and
31 activity-dependent manner remains unclear. Here we show that SUSD4, a complement-related
32 transmembrane protein, binds the AMPA receptor subunit GLUA2 and controls its activity-
33 dependent degradation. Several proteins with known roles in the regulation of AMPA receptor
34 turnover, in particular ubiquitin ligases of the NEDD4 subfamily, are identified as SUSD4 binding
35 partners. SUSD4 is expressed by many neuronal populations starting at the time of synapse
36 formation. Loss-of-function of *Susd4* in the mouse prevents long-term depression at cerebellar
37 synapses, and leads to impairment in motor coordination adaptation and learning. Our findings
38 reveal that activity-dependent synaptic plasticity relies on a transmembrane CCP domain-
39 containing protein that regulates the degradation of specific substrates. This mechanism potentially
40 accounts for the role of SUSD4 mutations in neurodevelopmental diseases.

41

42 **Introduction**

43

44 Proteostasis is at the core of many cellular processes and its dynamics needs to be finely regulated
45 for each protein in each organelle. In neurons, additional challenges are imposed by their spatial
46 complexity. In particular, during long-term synaptic plasticity, the proposed substrate for learning
47 and memory (Collingridge et al., 2010; Nicoll, 2017), the number of neurotransmitter receptors
48 needs to be regulated independently in a synapse-specific and activity-dependent manner. At
49 excitatory synapses, the modification of AMPA receptor numbers is a highly dynamic process,
50 involving regulation of receptor diffusion (Choquet and Triller, 2013; Penn et al., 2017), their
51 insertion in the plasma membrane, anchoring at the postsynaptic density and endocytosis
52 (Anggono and Huganir, 2012). After activity-dependent endocytosis, AMPA receptors are either
53 recycled to the plasma membrane or targeted to the endolysosomal compartment for degradation
54 (Ehlers, 2000; Lee et al., 2004; Park et al., 2004). The decision between these two fates, recycling
55 or degradation, regulates the direction of synaptic plasticity. Recycling promotes long-term
56 potentiation (LTP) and relies on many molecules, such as GRASP1, GRIP1, PICK1 and NSF
57 (Anggono and Huganir, 2012). Targeting to the endolysosomal compartment and degradation
58 promote long-term depression (LTD; Fernandez-Monreal et al., 2012; Kim et al., 2017; Matsuda
59 et al., 2013), but the regulation of the targeting and degradation process remains poorly understood.

60

61 The Complement Control Protein domain (CCP), an evolutionarily conserved module also known
62 as Sushi domain, was first characterized in proteins with role in immunity, in particular in the
63 complement system. In the past few years, proteins with CCP domains have been increasingly
64 recognized for their role at neuronal synapses. Acetylcholine receptor clustering is regulated by
65 CCP domain-containing proteins in *Caenorhabditis elegans* (Gendrel et al., 2009) and in
66 *Drosophila melanogaster* (Nakayama et al., 2016). In humans, mutations in the CCP domain-
67 containing secreted protein SRPX2 are associated with epilepsy and speech dysfunction, and
68 SRPX2 knockdown leads to decreased synapse number and vocalization in mice (Sia et al., 2013).
69 Recently SRPX2 has been involved in the regulation of synapse elimination in the visual and
70 somatosensory systems (Cong et al., 2020). Despite the increase in the diversity of CCP domain-
71 containing proteins in evolution (11 CCP domain-containing in *C. elegans* and 56 in humans;
72 smart.embl.de), the function of many CCP domain-containing proteins remains unknown.

73 The mammalian *SUSD4* gene codes for a transmembrane protein with four extracellular CCP
74 domains (**Figure 1A**) and is highly expressed in the central nervous system (Holmquist et al.,
75 2013). The *SUSD4* gene is located in a genomic region deleted in patients with the 1q41q42
76 syndrome that includes developmental delays and intellectual deficiency (ID; Rosenfeld et al.,
77 2011). *SUSD4* is also amongst the 124 genes enriched in *de novo* missense mutations in a large
78 cohort of individuals with Autism Spectrum Disorders (ASDs) or IDs (Coe et al., 2019). A copy
79 number variation and several *de novo* mutations with a high CADD score, which indicates the
80 deleteriousness of the mutations, have been described in the *SUSD4* gene in patients with ASDs
81 ((Cuscó et al., 2009); denovo-db, Seattle, WA (denovo-db.gs.washington.edu) 10, 2019). The
82 *SUSD4* protein has been described to regulate complement system activation in erythrocytes by
83 binding the C1Q globular domain (Holmquist et al., 2013). Interestingly, this domain is found in
84 major synaptic regulators such as C1QA (Stevens et al., 2007), CBLNs (Matsuda et al., 2010;

85 Uemura et al., 2010) and C1Q-like proteins (Bolliger et al., 2011; Kakegawa et al., 2015; Sigoillot
86 et al., 2015). Altogether these studies point to a potential role of SUSD4 in synapse formation
87 and/or function and in the etiology of neurodevelopmental disorders.

88 Proper development and function of the cerebellar circuitry is central for motor coordination and
89 adaptation, and a range of cognitive tasks (Badura et al., 2018; Hirai et al., 2005; Ichise et al.,
90 2000; Lefort et al., 2019; Rochefort et al., 2011; Tsai et al., 2012). Cerebellar dysfunction is
91 associated with several neurodevelopmental disorders including ASDs (Stoodley, 2016; Stoodley
92 et al., 2018; Wang et al., 2014). In this circuit, cerebellar Purkinje cells (PCs) receive more than a
93 hundred thousand parallel fiber (PF) synapses whose formation, maintenance and plasticity are
94 essential for cerebellar-dependent learning (Gutierrez-Castellanos et al., 2017; Hirai et al., 2005;
95 Ito, 2006; Kashiwabuchi et al., 1995). Postsynaptic LTD was first described at synapses between
96 PFs and cerebellar PCs (Gao et al., 2012; Hirano, 2018; Ito, 2001; Ito and Kano, 1982), where it
97 can be induced by conjunctive stimulation of PFs with the other excitatory input received by PCs,
98 the climbing fiber (CF; Coesmans et al., 2004; Ito, 2001; Suvrathan et al., 2016). The function of
99 members of the C1Q family, such as CBLN1 and C1QL1, is essential for excitatory synapse
100 formation and LTD in cerebellar PCs (Hirai et al., 2005; Kakegawa et al., 2015; Matsuda et al.,
101 2010; Sigoillot et al., 2015; Uemura et al., 2010), suggesting that proteins such as SUSD4, that
102 interact with the C1Q globular domain, could regulate these processes.

103 Gene expression studies from our laboratory revealed that *Susd4* is highly expressed in the
104 olivocerebellar system of the mouse. In order to uncover the potential link between SUSD4 and
105 neurodevelopmental disorders and the involvement of the olivocerebellar circuit in such diseases,
106 we sought to identify the role of SUSD4 in brain development and function, by analyzing the
107 phenotype of a *Susd4* loss-of-function mouse model in the cerebellum. Here we show that
108 knockout of the *Susd4* gene leads to misregulation of synaptic plasticity in cerebellar PCs, deficits
109 in motor coordination adaptation and learning as well as an impairment in the control of activity-
110 dependent degradation of GLUA2 AMPA receptor subunits. Using affinity-purification of
111 synaptosome preparations followed by proteomics analysis, we found that the SUSD4 protein
112 binds proteins that are involved in the regulation of several parameters controlling AMPA receptor
113 turnover. In particular, SUSD4 directly interacts with E3 ubiquitin ligases of the NEDD4 family,
114 which are known to regulate ubiquitination and degradation of their substrates. Finally, our results
115 suggest that SUSD4 promotes degradation of GLUA2 subunits over recycling at synapses, thereby
116 contributing to the decision between potentiation and depression. Given the domain structure of
117 SUSD4, this new regulatory mechanism could bring spatio-temporal specificity to the degradation
118 machinery in neurons, allowing proper synaptic plasticity and learning.

119

120 **Results**

121 ***Susd4* is broadly expressed in neurons during postnatal development**

122 Given the potential synaptic role for SUSD4, its pattern of expression should correlate with the
123 timing of synapse formation and/or maturation during postnatal development. *In situ* hybridization
124 experiments using mouse brain sections showed high expression of *Susd4* mRNA in neurons in
125 many regions of the central nervous system, including the cerebral cortex, the hippocampus, the
126 cerebellum and the brainstem (**Figure 1B** and **S1**). *Susd4* expression was already detected as early
127 as postnatal day 0 (P0) in some regions, but increased with brain maturation (**Figure S1**). In the
128 cerebellum, a structure where the developmental sequence leading to circuit formation and

129 maturation is well described (Sotelo, 2004), quantitative RT-PCR showed that *Susd4* mRNA levels
130 start increasing at P7 and by P21 reach about 15 times the levels detected at birth (**Figure 1B**). At
131 P7, a major increase in synaptogenesis is observed in the cerebellum. At this stage, hundreds of
132 thousands of PF excitatory synapses form on the distal dendritic spines of each PC, and a single
133 CF arising from an inferior olivary neuron translocates and forms about 300 excitatory synapses
134 on proximal PC dendrites (Leto et al., 2016). In the brainstem, where cell bodies of inferior olivary
135 neurons are located, the increase in *Susd4* mRNA expression occurs earlier, already by P3, and
136 reaches a peak by P14 (**Figure 1B**). Similarly to the cerebellum, this pattern of *Susd4* expression
137 parallels the rate of synaptogenesis that increases during the first postnatal week in the inferior
138 olive (Gotow and Sotelo, 1987). To identify the subcellular localization of the SUSD4 protein and
139 because of the lack of suitable antibodies for immunolabeling, viral particles enabling CRE-
140 dependent coexpression of HA-tagged SUSD4 and GFP in neurons were injected in the cerebellum
141 of adult mice expressing the CRE recombinase specifically in cerebellar PCs. Immunofluorescent
142 labeling against the HA tag demonstrated the localization of HA-SUSD4 in dendrites and in some
143 of the numerous dendritic spines present on the surface of distal dendrites (**Figure 1C**). These
144 spines are the postsynaptic compartments of PF synapses in PCs. Immunofluorescence analysis of
145 transduced cultured PCs further showed that HA-tagged SUSD4 could be immunolabeled in non-
146 permeabilizing conditions and located at the surface of dendrites and spines (**Figure 1D**). Double
147 labeling with the postsynaptic marker GLUR δ 2 (GRID2) further showed partial colocalization at
148 the surface of some, but not all, spines. Therefore, the timing of *Susd4* mRNA expression during
149 postnatal development and the subcellular localization of the SUSD4 protein in cerebellar PCs are
150 in agreement with a potential role for SUSD4 in excitatory synapse formation and/or function.

151

152 ***Susd4* loss-of-function leads to deficits in motor coordination and learning**

153 To determine the synaptic function of SUSD4, we analyzed the phenotype of *Susd4*^{-/-} constitutive
154 knockout (KO) mice with a deletion of exon 1 (**Figure 1E, 1G and S2**). RT-PCR using primers
155 encompassing the last exons and the 3'UTR show the complete absence of *Susd4* mRNA in the
156 brain of these *Susd4* KO mice (**Figure S2**). No obvious alterations of mouse development and
157 behavior were detected in those mutants, an observation that was confirmed by assessment of their
158 physical characteristics (weight, piloerection), basic behavioral abilities such as sensorimotor
159 reflexes (whisker responses, eye blinking) and motor responses (open field locomotion; cf. **Table**
160 **S1**). Because of the high expression of *Susd4* in the olivocerebellar system (**Figures 1G and S1**),
161 we further assessed the behavior of *Susd4* KO mice for two abilities well known to depend on
162 normal function of this network, motor coordination and motor learning (Kayakabe et al., 2014;
163 Lalonde and Strazielle, 2001; Rondi-Reig et al., 1997). Using a footprint test, a slightly larger print
164 separation of the front and hind paws in the *Susd4* KO mice was detected but no differences in the
165 stride length and stance width were found (**Figure S3**). In the accelerated rotarod assay, a classical
166 test of motor adaptation and learning (Buitrago et al., 2004), the mice were tested three times per
167 day at one hour interval during five consecutive days. The *Susd4* KO mice performed as well as
168 the *Susd4*^{+/+} (WT) littermate controls on the first trial (**Figure 1F, day 1, trial 1**). This indicates
169 that there is no deficit in their balance function, despite the slight change in fine motor coordination
170 found in the footprint test. However, while the control mice improved their performance as early
171 as the third trial on the first day, and further improved with several days of training, no learning
172 could be observed for the *Susd4* KO mice either during the first day, or in the following days

173 **(Figure 1F)**. These results show that *Susd4* loss-of-function leads to impaired motor coordination
174 and learning in adult mice.

175

176 ***Susd4* loss-of-function prevents long-term depression (LTD) at cerebellar parallel** 177 **fiber/Purkinje cell synapses**

178 Motor coordination and learning are deficient when cerebellar development is impaired (Hirai et
179 al., 2005; Ichise et al., 2000; Tsai et al., 2012; Zuo et al., 1997). No deficits in the global
180 cytoarchitecture of the cerebellum and morphology of PCs were found in *Susd4* KO mice (**Figure**
181 **S4**). Using high density microelectrode array, we assessed the spontaneous activity of PCs in acute
182 cerebellar slices from *Susd4* KO mice, and compared to *Susd4* WT mice (**Figure S5**). No
183 differences were detected in either the mean spiking frequency, the coefficient of variation of
184 interspike intervals (CV) and the intrinsic variability of spike trains (CV2, Holt and Douglas, 1996)
185 indicating that the firing properties of PCs are not affected by *Susd4* loss-of-function.

186 Co-immunolabeling of PF presynaptic boutons using an anti-VGLUT1 antibody and PCs using an
187 anti-calbindin antibody in cerebellar sections from juvenile WT mice revealed an extremely dense
188 staining in the molecular layer corresponding to the highly numerous PFs contacting PC distal
189 dendritic spines (**Figure 2A**). The labeling pattern appeared to be similar in *Susd4* KO. High-
190 resolution microscopy and quantitative analysis confirmed that there are no significant changes in
191 the mean density and volume of VGLUT1 clusters following *Susd4* loss-of-function (**Figure 2A**).
192 Electric stimulation of increasing intensity in the molecular layer allows the progressive
193 recruitment of PFs (Konnerth et al., 1990), and can be used to assess the number of synapses and
194 basic PF/PC transmission using whole-cell patch-clamp recordings of PCs on acute cerebellar
195 slices (**Figure 2B**). No difference was observed in the amplitude and the kinetics of the responses
196 to PF stimulation in PCs from *Susd4* KO and control littermate mice (**Figure 2C** and **Figure S6**).
197 Furthermore, the probability of vesicular release in the presynaptic PF boutons, as assessed by
198 measurements of paired pulse facilitation (Atluri and Regehr, 1996; Konnerth et al., 1990; Valera
199 et al., 2012), was not changed at PF/PC synapses (**Figure 2C**). Finally, no differences in the
200 frequency and amplitude of PF/PC evoked quantal events were detected (**Figure S6**). Thus, in
201 accordance with the morphological analysis, *Susd4* invalidation has no major effect on the number
202 and basal transmission of PF/PC synapses in the mouse.

203 Long-term synaptic plasticity of PF/PC synapses is involved in proper motor coordination and
204 adaptation learning (Gutierrez-Castellanos et al., 2017; Hirano, 2018; Kakegawa et al., 2018). We
205 first assessed LTD in PF/PC synapses using conjunctive stimulation of PFs and CFs and whole-
206 cell patch-clamp recordings of PCs in acute cerebellar slices from juvenile mice. The LTD
207 induction protocol produced a 42% average decrease in the amplitude of PF excitatory
208 postsynaptic currents (EPSCs) in PCs from WT mice while the paired pulse facilitation ratio was
209 not changed during the course of our recordings (**Figure 2D** and **Figure S6**). In *Susd4* KO PCs,
210 the same LTD induction protocol did not induce any significant change in PF EPSCs during the
211 30 minutes recording period, showing that LTD induction and maintenance are greatly impaired
212 in the absence of SUSD4 (**Figure 2D**). LTP can be induced by high frequency stimulation of PFs
213 only, and is also involved in cerebellar dependent-learning (Binda et al., 2016; Gutierrez-
214 Castellanos et al., 2017). In control mice, tetanic stimulation during 5 minutes induced a transient
215 increase in transmission of about 20% and the amplitude of the response returned to baseline after
216 only 15 minutes (**Figure 2E** and **Figure S6**). However, in the case of *Susd4* KO PCs, the same

217 protocol induced a 27% increase in transmission that was maintained after 35 minutes (**Figure**
218 **2E**), indicating a facilitation of LTP of PF/PC synapses in the absence of *Susd4* expression.

219 Lack of LTD of PF/PC synapses could arise from deficient CF/PC transmission. To test this
220 possibility, we first crossed the *Susd4* KO mice with the *Htr5b*-GFP BAC transgenic line
221 (http://gensat.org/MMRRC_report.jsp?founder_id=17735) expressing soluble GFP specifically in
222 inferior olivary neurons in the olivocerebellar system to visualize CFs. We found that CFs had a
223 normal morphology and translocated along the proximal dendrites of their PC target in *Susd4* KO
224 mice (**Figure 3A**). We then assessed whether developmental elimination of supernumerary CFs
225 was affected by *Susd4* invalidation using whole-cell patch-clamp recordings of PCs on cerebellar
226 acute slices (Crepel et al., 1976; Hashimoto and Kano, 2003). No difference was found in the
227 percentage of remaining multiply-innervated PCs in the absence of *Susd4* (**Figure 3B**). We next
228 used VGLUT2 immunostaining to label CF presynaptic boutons and analyze their morphology
229 using high resolution confocal microscopy and quantitative image analysis. VGLUT2
230 immunostaining revealed the typical CF innervation territory on PC proximal dendrites, extending
231 up to about 80% of the molecular layer height both in control *Susd4* WT and in *Susd4* KO mice
232 (**Figure 3C**). Furthermore, the number and density of VGLUT2 clusters were not significantly
233 different between *Susd4* WT and *Susd4* KO mice. To test whether the lack of CF-dependent PF
234 LTD was due to deficient CF transmission, we used whole-cell patch-clamp recordings of PCs in
235 acute cerebellar slices. Contrary to what could have been expected, the typical all-or-none CF
236 evoked EPSC was detected in PCs from *Susd4* KO mice with increased amplitude when compared
237 to WT PCs (**Figure 3D**) while no differences in CF-EPSC kinetics were found (**Figure S7**).
238 Therefore, the lack of CF-dependent PF/PC synapse LTD in *Susd4* KO mice is not due to impaired
239 CF/PC synapse formation or transmission. Measurements of evoked quantal events revealed an
240 increase in the amplitude of the quantal EPSCs at CF/PC synapses from juvenile mice (**Figures**
241 **3E** and **S7**). Paired-pulse facilitation and depression at PF/PC and CF/PC synapses, respectively,
242 are similar between *Susd4* KO and control mice, both in basal conditions and during plasticity
243 recordings (**Figures 2C, 3D, S6D** and **S6F**) suggesting strongly that the changes in PF/PC synaptic
244 plasticity and in CF/PC transmission in *Susd4* KO PCs have a postsynaptic origin. Overall our
245 results show that *Susd4* loss-of-function in mice leads to a highly specific phenotype characterized
246 by misregulation of postsynaptic plasticity in the absence of defects in synaptogenesis and in basal
247 transmission in cerebellar PCs.

248

249 ***Susd4* loss-of-function leads to deficient activity-dependent degradation of GLUA2**

250 What are the mechanisms that allow regulation of long-term synaptic plasticity by SUSD4? The
251 lack of LTD at PF/PC synapses and our analysis of evoked quantal events suggested the
252 involvement of SUSD4 in the regulation of postsynaptic receptor numbers. GLUA2 subunits are
253 present in most AMPA receptor channels in PC excitatory synapses (Masugi-Tokita et al., 2007;
254 Zhao et al., 1998). To assess whether *Susd4* loss-of-function leads to misregulation of the GLUA2
255 subunits at PC excitatory synapses, we first performed co-immunolabeling experiments using an
256 anti-GLUA2 antibody and an anti-VGLUT2 antibody on cerebellar sections followed by high-
257 resolution microscopy. Several GLUA2 clusters of varying sizes were detected in close association
258 with each VGLUT2 presynaptic cluster corresponding to a single CF release site, while very small
259 and dense GLUA2 clusters were found in the rest of the molecular layer which mostly correspond
260 to GLUA2 clusters at the PF/PC synapses (**Figure 4A**). No obvious change in GLUA2 distribution
261 in the molecular layer in *Susd4* KO mice was found when compared to controls, in accordance

262 with normal basal transmission in PF/PC synapses (**Figure 2C**). Quantitative analysis of the
263 GLUA2 clusters associated with VGLUT2 labelled CF presynaptic boutons did not reveal a
264 significant change in the total mean intensity of GLUA2 clusters per CF presynaptic bouton
265 (**Figure 4A**). However, the proportion of CF presynaptic boutons with no GLUA2 cluster was
266 smaller in juvenile *Susd4* KO mice than in WT mice (**Figure 4A**). This decrease partially explains
267 the increase in the amplitude of quantal EPSCs and CF transmission (**Figure 3E**).

268 In cerebellar PCs, regulation of the GLUA2 subunits at synapses and of their trafficking is essential
269 for PF LTD (Chung et al., 2003; Xia et al., 2000). To test whether activity-dependent surface
270 localization of GLUA2-containing AMPA receptors is affected by loss of *Susd4*, we set up a
271 biochemical assay in which we induced chemical LTD (cLTD) in acute cerebellar slices (Kim et
272 al., 2017) and performed surface biotinylation of GLUA2 subunits followed by immunoblot
273 quantification. As expected, our results showed a 35% mean reduction of surface GLUA2
274 receptors after cLTD in slices from WT mice (**Figure 4B**). In slices from *Susd4* KO mice, a similar
275 mean reduction of surface GLUA2 receptors was detected after cLTD (28%), suggesting that
276 SUSD4 does not affect the machinery controlling endocytosis of GLUA2 subunits.

277 Another parameter that needs to be controlled for proper LTD in PCs is the total number of AMPA
278 receptors in the recycling pool and the targeting of AMPA receptors to late endosomes and
279 lysosomes (Kim et al., 2017). Lack of LTD and facilitation of LTP in *Susd4* KO mice (**Figures**
280 **2D** and **2E**) suggest that GLUA2 activity-dependent targeting to the endolysosomal compartment
281 and its degradation is affected by *Susd4* loss-of-function. Using our cLTD assay in cerebellar
282 slices, we measured the total GLUA2 levels either in control conditions or in presence of inhibitors
283 of the proteasome (MG132) and of lysosomal degradation (leupeptin). The comparison of the
284 GLUA2 levels in the presence of both inhibitors and in control conditions allowed us to estimate
285 the GLUA2 degraded pool, regardless of the mechanism behind this degradation. On average, total
286 GLUA2 levels were not significantly different between *Susd4* WT and *Susd4* KO cerebellar slices
287 in basal conditions (**Figure S8**), in accordance with our morphological and electrophysiological
288 analysis of PF/PC synapses (**Figures 2A** and **2C**). In slices from WT mice, chemical induction of
289 LTD induced a significant reduction of 13% in total GLUA2 protein levels (**Figure 4C**). This
290 reduction was prevented by incubation with the mixture of degradation inhibitors, MG132 and
291 leupeptin, showing that it corresponds to the pool of GLUA2 degraded in an activity-dependent
292 manner (**Figure 4C**). In slices from *Susd4* KO mice, this activity-dependent degradation of
293 GLUA2 was completely absent. Additionally, the chemical induction of LTD had no effect on the
294 total protein levels of GLUR δ 2, another synaptic receptor highly present at PF/PC postsynaptic
295 densities, either in slices from WT or from *Susd4* KO mice (**Figure S8**). Thus, SUSD4 specifically
296 controls the activity-dependent degradation of GLUA2-containing AMPA receptors during LTD.

297 Finally, in order to assess the potential colocalization of SUSD4 and GLUA2 in neurons, we used
298 a Cre-dependent AAV construct to express HA-tagged SUSD4 in cultured PCs (**Figure 4D**) and
299 performed immunolabeling of surface GLUA2 subunits. Clusters of HA-tagged SUSD4 partially
300 colocalize with GLUA2 clusters at the surface of some dendritic spines (yellow arrowheads,
301 **Figure 4D**). Partial colocalization of GLUA2 and SUSD4 in neurons was also confirmed in
302 transfection experiments in hippocampal neurons (**Figure S9**). Altogether, these results suggest
303 that SUSD4 could regulate activity-dependent degradation of GLUA2-containing AMPA
304 receptors through a direct interaction.

305

306 **SUSD4 could regulate the number of AMPA receptor at synapses via multiple molecular**
307 **interactions**

308 To better understand how SUSD4 might regulate the number of GLUA2-containing AMPA
309 receptors at synapses, we searched for SUSD4 molecular partners by affinity-purification of
310 cerebellar synaptosome extracts using GFP-tagged SUSD4 as a bait (**Figure 5A**). Interacting
311 partners were identified by proteomic analysis using liquid chromatography with tandem mass
312 spectrometry (LC-MS/MS; Savas et al., 2014). 28 candidates were identified including proteins
313 with known function in the regulation of AMPA receptor turnover (**Figure 5E**). Several candidates
314 were functionally linked to ubiquitin ligase activity by gene ontology term analysis (**Figure 5A**
315 and **Table 1**). In particular, five members of the NEDD4 subfamily of HECT E3 ubiquitin ligases
316 were found as potential interacting partners, three of them (*Nedd4l*, *Wwp1* and *Itch*) exhibiting the
317 highest enrichment factors amongst the 28 candidates. Ubiquitination is a post-translational
318 modification essential for the regulation of protein turnover and trafficking in cells (Tai and
319 Schuman, 2008). A survey of the expression of HECT-ubiquitin ligases shows that different
320 members of the NEDD4 subfamily are broadly expressed in the mouse brain, however with only
321 partially overlapping patterns (**Figure S9**, <http://mouse.brain-map.org>, Allen Brain Atlas). *Nedd4*
322 and *Wwp1* are the most broadly expressed, including in neurons that also express *Susd4*, such as
323 hippocampal neurons, inferior olivary neurons in the brainstem and cerebellar PCs. SUSD4
324 interaction with NEDD4 ubiquitin ligases could thus participate in the control of synaptic plasticity
325 and of GLUA2 AMPA receptor subunit degradation. Immunoblot analysis of affinity-purified
326 synaptosome extracts confirmed the interaction of SUSD4 with NEDD4, ITCH and WWP1
327 (**Figure 5B**). Removal of the intracellular domain of SUSD4 (SUSD4 Δ C_T mutant) prevented this
328 interaction demonstrating the specificity of SUSD4 binding to NEDD4 ubiquitin ligases (**Figure**
329 **5B**).

330 One possibility is that SUSD4 binds directly to GLUA2 subunits to promote AMPA receptors
331 degradation and that the SUSD4 interactors modulate this function. In particular, the NEDD4
332 subfamily of HECT ubiquitin ligases is known to ubiquitinate and target for degradation many key
333 signaling molecules, including GLUA1- and GLUA2-containing AMPA receptors (Schwarz et al.,
334 2010; Widagdo et al., 2017). Ubiquitin ligases of the NEDD4 family bind variants of PY motifs
335 on target substrates and adaptors (Chen et al., 2017). However, GLUA1 and GLUA2 subunits lack
336 any obvious motif of this type. In contrast, two potential PY binding sites are present in the
337 intracellular domain of SUSD4 (**Figure 5C**).

338 To test whether SUSD4 interacts with GLUA2 and how this interaction might be affected by
339 SUSD4 binding to NEDD4 ubiquitin ligases, co-immunoprecipitation experiments were
340 performed on extracts from heterologous HEK293 cells transfected with SEP-tagged GLUA2 and
341 various HA-tagged SUSD4 constructs (**Figure 5C and 5D**). GLUA2 was detected in extracts
342 obtained after affinity-purification of the HA-tagged full length SUSD4 (HA-SUSD4), while it
343 was absent if HA-SUSD4 was replaced by a control transmembrane protein, PVRL3 α (**Figure**
344 **5D**). To test which domain in SUSD4 is responsible for this interaction, several deletion constructs
345 were generated (**Figure 5C**). Strong co-immunoprecipitation of GLUA2 was detected in affinity-
346 purified extracts from cells expressing the HA-tagged extracellular domain of SUSD4 alone (HA-
347 SUSD4-N_T construct), showing that this domain is sufficient for GLUA2 interaction. Deletion of
348 the extracellular domain (HA-SUSD4 Δ N_T) or of the cytoplasmic domain (HA-SUSD4 Δ C_T) of
349 SUSD4 did not abrogate binding to GLUA2, showing the cooperation of several domains of
350 SUSD4 for the binding to the GLUA2 subunit (**Figure 5D**). Furthermore, the level of GLUA2

351 recovered in extracts from HA-SUSD4 Δ C_T transfected cells was intermediate between the one
352 affinity-purified from HA-SUSD4-N_T and HA-SUSD4 transfected cells, suggesting that the
353 cytoplasmic domain of SUSD4 plays a regulatory role for GLUA2 binding.

354 To test whether the two PY motifs in the intracellular tail of SUSD4 mediate the binding of
355 NEDD4 ubiquitin ligases and whether mutations in these sites could change SUSD4's ability to
356 interact with GLUA2, we generated single- and double-point mutants. While the mutation of the
357 PPxY site (SUSD4- Δ PY mutant) abrogated binding of SUSD4 only partially, mutation of only the
358 LPxY site (SUSD4- Δ LY mutant) or of both sites (SUSD4- Δ PY/LY mutant) completely prevented
359 the binding to NEDD4 ubiquitin ligases (**Figures 5C and D**). These mutations did not change
360 significantly the level of SUSD4 protein in transfected HEK293 cells suggesting that the
361 degradation of SUSD4 itself is not regulated by NEDD4 ubiquitin ligases (**Figure S11**). The same
362 levels of SEP-GLUA2 were detected in affinity-purified samples whether HA-tagged full-length
363 SUSD4 or the point mutants unable to bind NEDD4 ubiquitin ligases were used as a bait (**Figure**
364 **5D**). This shows that interaction of NEDD4 ubiquitin ligases does not affect SUSD4's ability to
365 interact with GLUA2.

366 Overall, our results suggest that the interaction of SUSD4 with GLUA2 could directly promote its
367 activity-dependent degradation and that this function could be regulated by several molecular
368 partners (**Figure 5E**). In particular, direct interaction with NEDD4 ubiquitin ligases could either
369 promote GLUA2 ubiquitination in an activity-dependent manner in neurons or regulate the
370 interaction of SUSD4 with other pathways revealed by our proteomics analysis (**Figure 5E**).

371

372 **Discussion**

373 Our study shows that the CCP domain-containing protein SUSD4 starts to be expressed in various
374 neurons of the mammalian central nervous system when synapses are formed and mature. *Susd4*
375 loss-of-function in mice leads to impaired motor coordination adaptation and learning,
376 misregulation of synaptic plasticity in cerebellar PCs and deficient activity-dependent degradation
377 of GLUA2-containing AMPA receptors. SUSD4 can bind GLUA2 subunit and controls its
378 degradation. This function of SUSD4 could be regulated by its direct binding to ubiquitin ligases
379 of the NEDD4 family.

380

381 **SUSD4 promotes long-term synaptic depression**

382 The choice between recycling of AMPA receptors to the membrane or targeting to the
383 endolysosomal compartment for degradation is key for the regulation of the number of AMPA
384 receptors at synapses, as well as for the direction and degree of activity-dependent synaptic
385 plasticity (Ehlers, 2000; Lee et al., 2002). Blocking trafficking of AMPA receptors through
386 recycling endosomes, for example using a RAB11 mutant, prevents long-term potentiation (LTP)
387 in neurons (Park et al., 2004). Conversely, blocking the sorting of AMPA receptors to the
388 endolysosomal compartment, for example using a RAB7 mutant, impairs long-term depression
389 (LTD) in hippocampal CA1 pyramidal neurons and cerebellar Purkinje cells (PCs) (Fernandez-
390 Monreal et al., 2012; Kim et al., 2017). Further support for the role of receptor degradation comes
391 from mathematical modeling showing that in cerebellar PCs LTD depends on the regulation of the
392 total pool of glutamate receptors (Kim et al., 2017). The GLUA2 AMPA receptor subunit, and its
393 regulation, is of particular importance for LTD (Diering and Huganir, 2018). Phosphorylation in

394 its C-terminal tail and the binding of molecular partners such as PICK1 and GRIP1/2 is known to
395 regulate endocytosis and recycling (Bassani et al., 2012; Chiu et al., 2017; Fiuza et al., 2017), and
396 mutations in some of the phosphorylation sites leads to impaired LTD (Chung et al., 2003). The
397 molecular partners regulating the targeting for degradation of GLUA2 subunits in an activity-
398 dependent manner during LTD remain to be identified. Our study shows that loss-of-function of
399 *Susd4* leads both to loss of LTD and loss of activity-dependent degradation of GLUA2 subunits.
400 Loss-of-function of *Susd4* does not affect degradation of another postsynaptic receptor, GluD2,
401 showing the specificity of SUSD4 action. Furthermore, loss-of-function of *Susd4* facilitates LTP
402 of PF/PC synapses. Overall our results support a model in which, during LTD, a specific molecular
403 machinery containing SUSD4 promotes targeting of GLUA2-containing AMPA receptors to the
404 degradation compartment in an activity-dependent manner, away from the recycling pathway that
405 promotes LTP.

406

407 **SUSD4 might promote GLUA2 subunits targeting to the degradation compartment**

408 The degradation of specific targets such as neurotransmitter receptors must be regulated in a
409 stimulus-dependent and synapse-specific manner in neurons, to ensure proper long-term synaptic
410 plasticity, learning and memory (Tai and Schuman, 2008). How is this level of specificity
411 achieved? Adaptor proteins, such as GRASP1, GRIP1, PICK1 and NSF, are known to promote
412 AMPA receptor recycling and LTP (Anggono and Huganir, 2012). Such adaptors for the
413 promotion of LTD remain to be found.

414 Our results show that SUSD4 and GLUA2 AMPA receptor subunits interact in cells, colocalize in
415 neurons, and that SUSD4 promotes GLUA2 degradation. Furthermore, our affinity-purification
416 experiments identified SUSD4 as a binding partner for HECT E3 ubiquitin ligases of the NEDD4
417 family. The family of HECT E3 ubiquitin ligases contains 28 enzymes including the NEDD4
418 subfamily that is characterized by an N-terminal C2 domain, several WW domains and the
419 catalytic HECT domain (Weber et al., 2019). This subgroup of E3 ligases adds K63 ubiquitin
420 chains to their substrate, a modification that promotes sorting to the endolysosomal compartment
421 for degradation (Boase and Kumar, 2015). NEDD4 E3 ligases are highly expressed in neurons in
422 the mammalian brain and have many known substrates with various functions, including ion
423 channels and the GLUA1 AMPA receptor subunit. Accordingly, knockout mice for the *Nedd4-1*
424 gene die during late gestation (Kawabe et al., 2010). The activity and substrate selectivity of
425 NEDD4 E3 ligases thus need to be finely tuned. Both GLUA1 and GLUA2 AMPA receptor
426 subunits are ubiquitinated on lysine residues in their intracellular tails in an activity-dependent
427 manner (Lin et al., 2011; Lussier et al., 2011; Schwarz et al., 2010; Widagdo et al., 2015). Mutation
428 of these lysine residues decreases localization of GLUA1 and GLUA2 AMPA receptor subunits
429 in the endolysosomal compartment in neurons (Widagdo et al., 2015). However, GLUA1 and
430 GLUA2 subunits lack any obvious intracellular direct binding motif to the WW domain of NEDD4
431 ubiquitin ligases, raising questions about the precise mechanism allowing regulation of AMPA
432 subunits trafficking and degradation by these enzymes. SUSD4 could play a role in regulating
433 targeting of NEDD4 ubiquitin ligases to AMPA receptors in an activity-dependent manner in
434 neurons. Alternatively, the interaction of SUSD4 with NEDD4 ubiquitin ligases might regulate the
435 trafficking of the SUSD4/GLUA2 complex to the degradation pathway.

436 Further work is warranted to determine the mechanism of action of SUSD4 in neurons. In
437 particular how is the specificity of its action achieved and how is neuronal activity regulating this

438 pathway? Among the potential partners of SUSD4 identified by our proteomics analysis, several
439 encompass functions that are relevant for the regulation of synaptic plasticity, such as receptor
440 anchoring, clathrin mediated endocytosis and proteasome function (**Figure 5E**). Moreover, our
441 results suggest that not all spines contain SUSD4 and thus an attractive hypothesis is that its
442 recruitment to synapses is activity-dependent. However another possibility lies in activity-
443 dependent proteolysis, which has been shown to regulate the function of several types of cell
444 adhesion molecules (Shinoe and Goda, 2015). The presence of four CCP domains in the
445 extracellular region of SUSD4 suggests that it could bind proteins extracellularly. In particular, it
446 was previously shown that SUSD4 can bind the C1Q globular domain of the complement protein
447 C1 (Holmquist et al., 2013), a domain that is also found in presynaptic proteins of the C1Q family
448 known for their role in synapse formation and function (Sigoillot et al., 2015; Südhof, 2018;
449 Yuzaki, 2011). SUSD4 could thus enable fine spatiotemporal regulation of the degradation of
450 GLUA2-containing AMPA receptors in a trans-synaptic manner.

451

452 **SUSD4 and neurodevelopmental disorders**

453 In humans, the 1q41-42 deletion syndrome is characterized by many symptoms including IDs and
454 seizures, and in a high majority of the cases the microdeletion encompasses the *Susd4* gene
455 (Rosenfeld et al., 2011). A *Susd4* copy number variation has been identified in a patient with
456 autism spectrum disorder (ASD)(Cuscó et al., 2009). *Susd4* was recently identified amongst the
457 124 genes with genome wide significance for *de novo* mutations in a cohort of more than 10,000
458 patients with ASD or IDs (Coe et al., 2019). The *GRIA2* gene (coding for the GLUA2 subunit) has
459 been found as an ASD susceptibility gene (Salpietro et al., 2019; Satterstrom et al., 2018) and
460 mutations or misregulation of ubiquitin ligases have been found in many models of ASDs or
461 intellectual deficiencies (Cheon et al., 2018; Lee et al., 2018; Satterstrom et al., 2018). For
462 example, ubiquitination of GLUA1 by NEDD4-2 is impaired in neurons from a model of Fragile
463 X syndrome (Lee et al., 2018). Understanding the precise molecular mechanisms underlying the
464 activity-dependent degradation of GLUA2 by the SUSD4/NEDD4 complex will thus be of
465 particular importance for our understanding of the etiology of these neurodevelopmental disorders.

466 Mutations in the *Susd4* gene might contribute to the etiology of neurodevelopmental disorders by
467 impairing synaptic plasticity. Deficits in LTD such as the one found in the *Susd4* KO mice are a
468 common feature of several mouse models of ASDs (Auerbach et al., 2011; Baudouin et al., 2012;
469 Piochon et al., 2014). *Susd4* loss-of-function leads to motor impairments, a symptom that is also
470 found in ASD patients (Fournier et al., 2010). Very recently, a reduction in exploratory behavior,
471 in addition to impairments of motor coordination, was reported after *Susd4* loss-of-function (Zhu
472 et al., 2020). Long-term synaptic plasticity has been proposed as a mechanism for learning and
473 memory. While *in vivo* evidence for the role of LTP in these processes has accumulated, the role
474 of LTD is still discussed (Andersen et al., 2017; Kakegawa et al., 2018; Raymond and Medina,
475 2018; Schonewille et al., 2011). Because of the broad expression of SUSD4 and of ubiquitin ligases
476 of the NEDD4 subfamily in the mammalian central nervous system, this pathway is likely to
477 control synaptic plasticity at many synapse types and its misregulation might lead to impairments
478 in many learning and memory paradigms.

479

480

481 **Acknowledgments:** We gratefully acknowledge the Collège de France imaging facility
482 (IMACHEM-IBiSA), in particular P. Mailly for help with the design of the macro for GLUA2
483 quantification and Estelle Anceaume for help with image acquisition. We also thank the personnel
484 from the CIRB, INCI and chronobiotron CNRS UMS 3415, IBPS and IBENS animal facilities.
485 We would like to thank Philippe Marin for advice on proteomics analysis. Mass spectrometry
486 experiments were carried out using facilities of the Functional Proteomics Platform of Montpellier.
487 **Funding:** This work was supported by funding from: ATIP-AVENIR program (RSE11005JSA to
488 FS), Idex PSL ANR-10-IDEX-0001-02 PSL*(FS), ANR 9139SAMA90010901 (to FS and PI),
489 ANR-15-CE37-0001-01 CeMod (to PI and FS), Fondation pour la Recherche Médicale Equipe
490 FRM DEQ20150331748 (FS) and DEQ20140329514 (PI), and European Research Council ERC
491 consolidator grant SynID 724601 (to FS). KI was supported by a PhD grant from the Ecole des
492 Neurosciences de Paris (ENP) and the ENS Labex MemoLife (ANR-10-LABX-54 MEMO LIFE).
493 JV and LR-R were supported by ANR-10-LABX-BioPsy (ANR-11-IDEX-0004-02) and ENP
494 Foundation.

495
496 **Contributions:** FS, PI, LR-R, IG-C and KI designed the study and the experiments. IG-C, KI,
497 MC, AK, FAG, JV, MS, ST, MA, OV, YN, AD, FS, SMS, MV and CB-L performed the
498 experiments, and collected the data; AT and J-LB provided the SUS4 knockout mice and
499 conceptual advice; FS and IG-C wrote the first draft of the manuscript; all authors read the
500 manuscript and KI, MC, AK, MS, SMS, CB-L, MV, AD, J-LB, PI and LR-R revised the
501 manuscript.

502
503 **Competing interests:** Authors declare no competing interests.

504 **Data and materials availability:** All data is available in the main text or the supplementary
505 materials.

506 **Supplementary Information:**

507 Materials and Methods

508 Figs. S1 to S11

509 Tables S1

510

511 **References**

512 Andersen N, Krauth N, Nabavi S. 2017. Hebbian plasticity in vivo: relevance and induction.

513 *Curr Opin Neurobiol.* doi:10.1016/j.conb.2017.06.001

514 Anggono V, Huganir RL. 2012. Regulation of AMPA receptor trafficking and synaptic

515 plasticity. *Curr Opin Neurobiol* **22**:461–469. doi:10.1016/j.conb.2011.12.006

516 Atluri PP, Regehr WG. 1996. Determinants of the Time Course of Facilitation at the Granule

517 Cell to Purkinje Cell Synapse. *J Neurosci* **16**:5661–5671.

518 Auerbach BD, Osterweil EK, Bear MF. 2011. Mutations causing syndromic autism define an

519 axis of synaptic pathophysiology. *Nature* **480**:63–68. doi:10.1038/nature10658

520 Badura A, Verpeut JL, Metzger JW, Pereira TD, Pisano TJ, Deverett B, Bakshinskaya DE, Wang

521 SS-H. 2018. Normal cognitive and social development require posterior cerebellar activity.

522 *Elife* **7**:1–36. doi:10.7554/eLife.36401

- 523 Bassani S, Cingolani LA, Valnegri P, Folci A, Zapata J, Gianfelice A, Sala C, Goda Y, Passafaro
524 M. 2012. The X-Linked Intellectual Disability Protein TSPAN7 Regulates Excitatory
525 Synapse Development and AMPAR Trafficking. *Neuron* **73**:1143–1158.
526 doi:10.1016/j.neuron.2012.01.021
- 527 Baudouin SJ, Gaudias J, Gerharz S, Hatstatt L, Zhou K, Punnakkal P, Tanaka KF, Spooren W,
528 Hen R, De Zeeuw CI, Vogt K, Scheiffele P. 2012. Shared synaptic pathophysiology in
529 syndromic and nonsyndromic rodent models of autism. *Science (80-)*.
530 doi:10.1126/science.1224159
- 531 Binda F, Dorgans K, Reibel S, Sakimura K, Kano M, Poulain B, Isope P. 2016. Inhibition
532 promotes long-Term potentiation at cerebellar excitatory synapses. *Sci Rep* **6**:1–12.
533 doi:10.1038/srep33561
- 534 Boase NA, Kumar S. 2015. NEDD4: The founding member of a family of ubiquitin-protein
535 ligases. *Gene* **557**:113–122. doi:10.1016/j.gene.2014.12.020
- 536 Bolliger MF, Martinelli DC, Sudhof TC. 2011. The cell-adhesion G protein-coupled receptor
537 BAI3 is a high-affinity receptor for C1q-like proteins. *Proc Natl Acad Sci* **108**:2534–2539.
538 doi:10.1073/pnas.1019577108
- 539 Buitrago MM, Schulz JB, Dichgans J, Luft AR. 2004. Short and long-term motor skill learning
540 in an accelerated rotarod training paradigm. *Neurobiol Learn Mem* **81**:211–216.
541 doi:10.1016/j.nlm.2004.01.001
- 542 Chen Z, Jiang H, Xu W, Li X, Dempsey DR, Zhang X, Devreotes P, Wolberger C, Amzel LM,
543 Gabelli SB, Cole PA. 2017. A Tunable Brake for HECT Ubiquitin Ligases. *Mol Cell*
544 **66**:345-357.e6. doi:10.1016/j.molcel.2017.03.020
- 545 Cheon S, Dean M, Chahrour M. 2018. The ubiquitin proteasome pathway in neuropsychiatric
546 disorders. *Neurobiol Learn Mem* 106791. doi:10.1016/j.nlm.2018.01.012
- 547 Chiu SL, Diering GH, Ye B, Takamiya K, Chen CM, Jiang Y, Niranjana T, Schwartz CE, Wang
548 T, Hugarir RL. 2017. GRASP1 Regulates Synaptic Plasticity and Learning through
549 Endosomal Recycling of AMPA Receptors. *Neuron* **93**:1405-1419.e8.
550 doi:10.1016/j.neuron.2017.02.031
- 551 Choquet D, Triller A. 2013. The dynamic synapse. *Neuron* **80**:691–703.
552 doi:10.1016/j.neuron.2013.10.013
- 553 Chung HJ, Steinberg JP, Hugarir RL, Linden DJ. 2003. Requirement of AMPA receptor GluR2
554 phosphorylation for cerebellar long-term depression. *Science (80-)* **300**:1751–1755.
555 doi:10.1126/science.1082915
- 556 Coe BP, Stessman HAF, Sulovari A, Geisheker MR, Bakken TE, Lake AM, Dougherty JD, Lein
557 ES, Hormozdiari F, Bernier RA, Eichler EE. 2019. Neurodevelopmental disease genes
558 implicated by de novo mutation and copy number variation morbidity. *Nat Genet* **51**:106–
559 116. doi:10.1038/s41588-018-0288-4
- 560 Coesmans M, Weber JT, De Zeeuw CI, Hansel C. 2004. Bidirectional parallel fiber plasticity in
561 the cerebellum under climbing fiber control. *Neuron* **44**:691–700.
562 doi:10.1016/j.neuron.2004.10.031
- 563 Collingridge GL, Peineau S, Howland JG, Wang YT. 2010. Long-term depression in the CNS.

- 564 *Nat Rev Neurosci* **11**:459–473. doi:10.1038/nrn2867
- 565 Cong Q, Soteros BM, Wollet M, Kim JH, Sia GM. 2020. The endogenous neuronal complement
566 inhibitor SRPX2 protects against complement-mediated synapse elimination during
567 development. *Nat Neurosci*. doi:10.1038/s41593-020-0672-0
- 568 Crepel F, Mariani J, Delhaye-Bouchaud N. 1976. Evidence for a multiple innervation of purkinje
569 cells by climbing fibers in the immature rat cerebellum. *J Neurobiol* **7**:567–578.
570 doi:10.1002/neu.480070609
- 571 Cuscó I, Medrano A, Gener B, Vilardell M, Gallastegui F, Villa O, González E, Rodríguez-
572 Santiago B, Vilella E, Del Campo M, Pérez-Jurado LA. 2009. Autism-specific copy number
573 variants further implicate the phosphatidylinositol signaling pathway and the glutamatergic
574 synapse in the etiology of the disorder. *Hum Mol Genet* **18**:1795–1804.
575 doi:10.1093/hmg/ddp092
- 576 Diering GH, Hugarir RL. 2018. The AMPA Receptor Code of Synaptic Plasticity. *Neuron*
577 **100**:314–329. doi:10.1016/j.neuron.2018.10.018
- 578 Ehlers MD. 2000. Reinsertion or degradation of AMPA receptors determined by activity-
579 dependent endocytic sorting. *Neuron* **28**:511–525. doi:10.1016/S0896-6273(00)00129-X
- 580 Fernandez-Monreal M, Brown TC, Royo M, Esteban JA. 2012. The Balance between Receptor
581 Recycling and Trafficking toward Lysosomes Determines Synaptic Strength during Long-
582 Term Depression. *J Neurosci* **32**:13200–13205. doi:10.1523/JNEUROSCI.0061-12.2012
- 583 Fiuza M, Rostosky C, Parkinson G, Bygrave A, Halemani N, Baptista M, Milosevic I, Hanley
584 JG. 2017. PICK1 regulates AMP receptor endocytosis via direct interaction with AP2 a-
585 appendage and dynamin. *Rockefeller Univ Press J Cell Biol* **216**:3323–3338.
586 doi:10.1083/jcb.201701034
- 587 Fournier KA, Hass CJ, Naik SK, Lodha N, Cauraugh JH. 2010. Motor coordination in autism
588 spectrum disorders: A synthesis and meta-analysis. *J Autism Dev Disord* **40**:1227–1240.
589 doi:10.1007/s10803-010-0981-3
- 590 Gao Z, Van Beugen BJ, De Zeeuw CI. 2012. Distributed synergistic plasticity and cerebellar
591 learning. *Nat Rev Neurosci*. doi:10.1038/nrn3312
- 592 Gendrel M, Rapti G, Richmond JE, Bessereau J-L. 2009. A secreted complement-control-related
593 protein ensures acetylcholine receptor clustering. *Nature* **461**:992–996.
594 doi:10.1038/nature08430
- 595 Gotow T, Sotelo C. 1987. Postnatal development of the inferior olivary complex in the rat: IV.
596 Synaptogenesis of GABAergic afferents, analyzed by glutamic acid decarboxylase
597 immunocytochemistry. *J Comp Neurol* **263**:526–552. doi:10.1002/cne.902630406
- 598 Gutierrez-Castellanos N, Da Silva-Matos CM, Zhou K, Canto CB, Renner MC, Koene LMC,
599 Ozyildirim O, Sprengel R, Kessels HW, De Zeeuw CI. 2017. Motor Learning Requires
600 Purkinje Cell Synaptic Potentiation through Activation of AMPA-Receptor Subunit GluA3.
601 *Neuron* **93**:409–424. doi:10.1016/j.neuron.2016.11.046
- 602 Hashimoto K, Kano M. 2003. Functional differentiation of multiple climbing fiber inputs during
603 synapse elimination in the developing cerebellum. *Neuron* **38**:785–796. doi:10.1016/S0896-
604 6273(03)00298-8

- 605 Hirai H, Pang Z, Bao D, Miyazaki T, Li L, Miura E, Parris J, Rong Y, Watanabe M, Yuzaki M,
606 Morgan JI. 2005. Cbln1 is essential for synaptic integrity and plasticity in the cerebellum.
607 *Nat Neurosci* **8**:1534–1541. doi:10.1038/nn1576
- 608 Hirano T. 2018. Regulation and Interaction of Multiple Types of Synaptic Plasticity in a Purkinje
609 Neuron and Their Contribution to Motor Learning. *Cerebellum* **17**:756–765.
- 610 Holmquist E, Okroj M, Nodin B, Jirström K, Blom AM. 2013. Sushi domain-containing protein
611 4 (SUSD4) inhibits complement by disrupting the formation of the classical C3 convertase.
612 *FASEB J* **27**:2355–2366. doi:10.1096/fj.12-222042
- 613 Holt GR, Douglas J. 1996. Comparison of Discharge Variability Visual Cortex Neurons. *J*
614 *Neurophysiol* **75**:1806–1814.
- 615 Ichise T, Kano M, Hashimoto K, Yanagihara D, Nakao K, Shigemoto R, Katsuki M, Aiba a.
616 2000. mGluR1 in cerebellar Purkinje cells essential for long-term depression, synapse
617 elimination, and motor coordination. *Science* **288**:1832–1835.
618 doi:10.1126/science.288.5472.1832
- 619 Ito M. 2006. Cerebellar circuitry as a neuronal machine. *Prog Neurobiol* **78**:272–303.
620 doi:10.1016/j.pneurobio.2006.02.006
- 621 Ito M. 2001. Cerebellar Long-Term Depression: Characterization, Signal Transduction, and
622 Functional Roles. *Physiol Rev* **81**:1143–1195. doi:10.1152/physrev.2001.81.3.1143
- 623 Ito M, Kano M. 1982. Long-lasting depression of parallel fiber-Purkinje cell transmission
624 induced by conjunctive stimulation of parallel fibers and climbing fibers in the cerebellar
625 cortex. *Neurosci Lett* **33**:253–258. doi:10.1016/0304-3940(82)90380-9
- 626 Kakegawa W, Katoh A, Narumi S, Miura E, Motohashi J, Takahashi A, Kohda K, Fukazawa Y,
627 Yuzaki M, Matsuda S. 2018. Optogenetic Control of Synaptic AMPA Receptor Endocytosis
628 Reveals Roles of LTD in Motor Learning. *Neuron* **99**:985-998.e6.
629 doi:10.1016/j.neuron.2018.07.034
- 630 Kakegawa W, Mitakidis N, Miura E, Abe M, Matsuda K, Takeo YH, Kohda K, Motohashi J,
631 Takahashi A, Nagao S, Muramatsu S ichi, Watanabe M, Sakimura K, Aricescu AR, Yuzaki
632 M. 2015. Anterograde Clq11 signaling is required in order to determine and maintain a
633 single-winner climbing fiber in the mouse cerebellum. *Neuron* **85**:316–330.
634 doi:10.1016/j.neuron.2014.12.020
- 635 Kashiwabuchi N, Ikeda K, Araki K, Hirano T, Shibuki K, Takayama C, Inoue Y, Kutsuwada T,
636 Yagi T, Kang Y, Aizawa S, Mishina M. 1995. Impairment of Motor Coordination, Purkinje
637 Cell Synapse Formation, and Cerebellar Long-Term Depression in GluRd2 Mutant Mice.
638 *Cell* **81**:245–252.
- 639 Kawabe H, Neeb A, Dimova K, Young SM, Takeda M, Katsurabayashi S, Mitkovski M,
640 Malakhova OA, Zhang DE, Umikawa M, Kariya K ichi, Goebbels S, Nave KA, Rosenmund
641 C, Jahn O, Rhee JS, Brose N. 2010. Regulation of Rap2A by the Ubiquitin Ligase Nedd4-1
642 Controls Neurite Development. *Neuron* **65**:358–372. doi:10.1016/j.neuron.2010.01.007
- 643 Kayakabe M, Kakizaki T, Kaneko R, Sasaki A, Nakazato Y, Shibasaki K, Ishizaki Y, Saito H,
644 Suzuki N, Furuya N, Yanagawa Y. 2014. Motor dysfunction in cerebellar Purkinje cell-
645 specific vesicular GABA transporter knockout mice. *Front Cell Neurosci* **7**:1–11.

- 646 doi:10.3389/fncel.2013.00286
- 647 Kim T, Yamamoto Y, Tanaka-Yamamoto K. 2017. Timely regulated sorting from early to late
648 endosomes is required to maintain cerebellar long-term depression. *Nat Commun* **8**.
649 doi:10.1038/s41467-017-00518-3
- 650 Konnerth A, Llanot I, Armstrong CM. 1990. Synaptic currents in cerebellar Purkinje cells.
651 *Neurobiology* **87**:2662–2665. doi:10.1073/pnas.87.7.2662
- 652 Lalonde R, Strazielle C. 2001. Motor performance and regional brain metabolism of spontaneous
653 murine mutations with cerebellar atrophy **125**:103–108.
- 654 Lee KY, Jewett KA, Chung HJ, Tsai NP. 2018. Loss of fragile X protein FMRP impairs
655 homeostatic synaptic downscaling through tumor suppressor p53 and ubiquitin E3 ligase
656 Nedd4-2. *Hum Mol Genet* **27**:2805–2816. doi:10.1093/hmg/ddy189
- 657 Lee SH, Liu L, Wang YT, Sheng M. 2002. Clathrin adaptor AP2 and NSF interact with
658 overlapping sites of GluR2 and play distinct roles in AMPA receptor trafficking and
659 hippocampal LTD. *Neuron* **36**:661–674. doi:10.1016/S0896-6273(02)01024-3
- 660 Lee SH, Simonetta A, Sheng M. 2004. Subunit rules governing the sorting of internalized AMPA
661 receptors in hippocampal neurons. *Neuron* **43**:221–236. doi:10.1016/j.neuron.2004.06.015
- 662 Lefort JM, Vincent J, Tallot L, Jarlier F, De Zeeuw CI, Rondi-Reig L, Rochefort C. 2019.
663 Impaired cerebellar Purkinje cell potentiation generates unstable spatial map orientation and
664 inaccurate navigation. *Nat Commun* **10**:1–13. doi:10.1038/s41467-019-09958-5
- 665 Leto K, Arancillo M, Becker EBE, Buffo A, Chiang C, Ding B, Dobyns WB, Dusart I, Haldipur
666 P, Hatten ME, Hoshino M, Joyner AL, Kano M, Kilpatrick DL, Koibuchi N, Marino S,
667 Martinez S, Millen KJ, Millner TO, Miyata T, Parmigiani E, Schilling K, Sekerková G,
668 Sillitoe R V., Sotelo C, Uesaka N, Wefers A, Wingate RJT, Hawkes R. 2016. Consensus
669 Paper: Cerebellar Development. *The Cerebellum* **15**:789–828. doi:10.1007/s12311-015-
670 0724-2
- 671 Lin A, Hou Q, Jarzylo L, Amato S, Gilbert J, Shang F, Man HY. 2011. Nedd4-mediated AMPA
672 receptor ubiquitination regulates receptor turnover and trafficking. *J Neurochem* **119**:27–39.
673 doi:10.1111/j.1471-4159.2011.07221.x
- 674 Lussier MP, Nasu-Nishimura Y, Roche KW. 2011. Activity-dependent ubiquitination of the
675 AMPA receptor subunit GluA2. *J Neurosci* **31**:3077–3081. doi:10.1523/JNEUROSCI.5944-
676 10.2011
- 677 Masugi-Tokita M, Tarusawa E, Watanabe M, Molnár E, Fujimoto K, Shigemoto R. 2007.
678 Number and density of AMPA receptors in individual synapses in the rat cerebellum as
679 revealed by SDS-digested freeze-fracture replica labeling. *J Neurosci* **27**:2135–2144.
680 doi:10.1523/JNEUROSCI.2861-06.2007
- 681 Matsuda K, Miura E, Miyazaki T, Kakegawa W, Emi K, Narumi S, Fukazawa Y, Ito-Ishida A,
682 Kondo T, Shigemoto R, Watanabe M, Yuzaki M. 2010. Cbln1 is a ligand for an orphan
683 glutamate receptor delta2, a bidirectional synapse organizer. *Science* **328**:363–368.
- 684 Matsuda S, Kakegawa W, Budisantoso T, Nomura T, Kohda K, Yuzaki M. 2013. Stargazin
685 regulates AMPA receptor trafficking through adaptor protein complexes during long-term
686 depression. *Nat Commun* **4**:1–15. doi:10.1038/ncomms3759

- 687 Nakayama M, Suzuki E, Tsunoda S -i., Hama C. 2016. The Matrix Proteins Hasp and Hig
688 Exhibit Segregated Distribution within Synaptic Clefts and Play Distinct Roles in
689 Synaptogenesis. *J Neurosci* **36**:590–606. doi:10.1523/JNEUROSCI.2300-15.2016
- 690 Nicoll RA. 2017. A Brief History of Long-Term Potentiation. *Neuron* **93**:281–290.
691 doi:10.1016/j.neuron.2016.12.015
- 692 Park M, Penick E, Edwards J, Kauer J, Ehlers MD. 2004. Recycling Endosomes Supply AMPA
693 Receptors for Long-term Potentiation. *Science (80-)* **305**:1972–1975.
- 694 Penn AC, Zhang CL, Georges F, Royer L, Breillat C, Hosity E, Petersen JD, Humeau Y, Choquet
695 D. 2017. Hippocampal LTP and contextual learning require surface diffusion of AMPA
696 receptors. *Nature* **549**:384–388. doi:10.1038/nature23658
- 697 Piochon C, Kloth AD, Grasselli G, Titley HK, Nakayama H, Hashimoto K, Wan V, Simmons
698 DH, Eissa T, Nakatani J, Cherskov A, Miyazaki T, Watanabe M, Takumi T, Kano M, Wang
699 SSH, Hansel C. 2014. Cerebellar plasticity and motor learning deficits in a copy-number
700 variation mouse model of autism. *Nat Commun* **5**:1–12. doi:10.1038/ncomms6586
- 701 Raymond JL, Medina JF. 2018. Computational Principles of Supervised Learning in the
702 Cerebellum. *Annu Rev Neurosci* **41**:233–253. doi:10.1146/annurev-neuro-080317-061948
- 703 Rochefort C, Arabo A, Andre M, Poucet B, Save E, Rondi-Reig L. 2011. Cerebellum Shapes
704 Hippocampal Spatial Code. *Science (80-)* **334**:385–389.
- 705 Rondi-Reig L, Delhaye-Bouchaud N, Mariani J, Caston J. 1997. Role of the inferior olivary
706 complex in motor skills and motor learning in the adult rat. *Neuroscience* **77**:955–963.
707 doi:10.1016/S0306-4522(96)00518-0
- 708 Rosenfeld JA, Lacassie Y, El-Khechen D, Escobar LF, Reggin J, Heuer C, Chen E, Jenkins LS,
709 Collins AT, Zinner S, Babcock M, Morrow B, Schultz RA, Torchia BS, Ballif BC,
710 Tsuchiya KD, Shaffer LG. 2011. New cases and refinement of the critical region in the
711 1q41q42 microdeletion syndrome. *Eur J Med Genet* **54**:42–49.
712 doi:10.1016/j.ejmg.2010.10.002
- 713 Salpietro V, Dixon CL, Guo H, Bello OD, Vandrovцова J, Efthymiou S, Maroofian R, Heimer
714 G, Burglen L, Valence S, Torti E, Hacke M, Rankin J, Tariq H, Colin E, Procaccio V,
715 Striano P, Mankad K, Lieb A, Chen S, Pisani L, Bettencourt C, Männikkö R, Manole A,
716 Brusco A, Grosso E, Ferrero GB, Armstrong-Moron J, Gueden S, Bar-Yosef O, Tzadok M,
717 Monaghan KG, Santiago-Sim T, Person RE, Cho MT, Willaert R, Yoo Y, Chae JH, Quan
718 Y, Wu H, Wang T, Bernier RA, Xia K, Blesson A, Jain M, Motazacker MM, Jaeger B,
719 Schneider AL, Boysen K, Muir AM, Myers CT, Gavrilova RH, Gunderson L, Schultz-
720 Rogers L, Klee EW, Dymont D, Osmond M, Parellada M, Llorente C, Gonzalez-Peñas J,
721 Carracedo A, Van Haeringen A, Ruivenkamp C, Nava C, Heron D, Nardello R, Iacomino
722 M, Minetti C, Skabar A, Fabretto A, Hanna MG, Bugiardini E, Hostettler I, O’Callaghan B,
723 Khan A, Cortese A, O’Connor E, Yau WY, Bourinaris T, Kaiyrzhanov R, Chelban V,
724 Madej M, Diana MC, Vari MS, Pedemonte M, Bruno C, Balagura G, Scala M, Fiorillo C,
725 Nobili L, Malintan NT, Zanetti MN, Krishnakumar SS, Lignani G, Jepson JEC, Broda P,
726 Baldassari S, Rossi P, Fruscione F, Madia F, Traverso M, De-Marco P, Pérez-Dueñas B,
727 Munell F, Kriouile Y, El-Khorassani M, Karashova B, Avdjieva D, Kathom H, Tincheva R,
728 Van-Maldergem L, Nachbauer W, Boesch S, Gagliano A, Amadori E, Goraya JS, Sultan T,
729 Kirmani S, Ibrahim S, Jan F, Mine J, Banu S, Veggiotti P, Zuccotti G V., Ferrari MD, Van

- 730 Den Maagdenberg AMJ, Verrotti A, Marseglia GL, Savasta S, Soler MA, Scuderi C,
731 Borgione E, Chimenz R, Gitto E, Dipasquale V, Sallemi A, Fusco M, Cuppari C, Cutrupi
732 MC, Ruggieri M, Cama A, Capra V, Mencacci NE, Boles R, Gupta N, Kabra M, Papacostas
733 S, Zamba-Papanicolaou E, Dardiotis E, Maqbool S, Rana N, Atawneh O, Lim SY, Shaikh
734 F, Koutsis G, Breza M, Coviello DA, Dauvilliers YA, AlKhawaja I, AlKhawaja M, Al-
735 Mutairi F, Stojkovic T, Ferrucci V, Zollo M, Alkuraya FS, Kinali M, Sherifa H, Benrhouma
736 H, Turki IBY, Tazir M, Obeid M, Bakhtadze S, Saadi NW, Zaki MS, Triki CC, Benfenati F,
737 Gustincich S, Kara M, Belcastro V, Specchio N, Capovilla G, Karimiani EG, Salih AM,
738 Okubadejo NU, Ojo OO, Oshinaike OO, Oguntunde O, Wahab K, Bello AH, Abubakar S,
739 Obiabo Y, Nwazor E, Ekenze O, Williams U, Iyagba A, Taiwo L, Komolafe M, Senkevich
740 K, Shashkin C, Zharkynbekova N, Koneyev K, Manizha G, Isrofilov M, Guliyeva U,
741 Salayev K, Khachatryan S, Rossi S, Silvestri G, Haridy N, Ramenghi LA, Xiromerisiou G,
742 David E, Aguenouz M, Fidani L, Spanaki C, Tucci A, Raspall-Chaure M, Chez M, Tsai A,
743 Fassi E, Shinawi M, Constantino JN, De Zorzi R, Fortuna S, Kok F, Keren B, Bonneau D,
744 Choi M, Benzeev B, Zara F, Mefford HC, Scheffer IE, Clayton-Smith J, Macaya A,
745 Rothman JE, Eichler EE, Kullmann DM, Houlden H. 2019. AMPA receptor GluA2 subunit
746 defects are a cause of neurodevelopmental disorders. *Nat Commun* **10**. doi:10.1038/s41467-
747 019-10910-w
- 748 Satterstrom FK, Kosmicki JA, Wang J, Breen MS. 2018. Large-scale exome sequencing study
749 implicates both developmental and functional changes in the neurobiology of autism 1–43.
- 750 Savas JN, De Wit J, Comoletti D, Zemla R, Ghosh A, Yates JR. 2014. Ecto-Fc MS identifies
751 ligand-receptor interactions through extracellular domain Fc fusion protein baits and
752 shotgun proteomic analysis. *Nat Protoc* **9**:2061–74. doi:10.1038/nprot.2014.140
- 753 Schonewille M, Gao Z, Boele HJ, Vinueza Veloz MF, Amerika WE, Šimek AAM, De Jeu MT,
754 Steinberg JP, Takamiya K, Hoebeek FE, Linden DJ, Hugarir RL, De Zeeuw CI. 2011.
755 Reevaluating the Role of LTD in Cerebellar Motor Learning. *Neuron* **70**:43–50.
756 doi:10.1016/j.neuron.2011.02.044
- 757 Schwarz LA, Hall BJ, Patrick GN. 2010. Activity-dependent ubiquitination of GluA1 mediates a
758 distinct AMPA receptor endocytosis and sorting pathway. *J Neurosci* **30**:16718–16729.
759 doi:10.1523/JNEUROSCI.3686-10.2010
- 760 Shinoe T, Goda Y. 2015. Tuning synapses by proteolytic remodeling of the adhesive surface.
761 *Curr Opin Neurobiol*. doi:10.1016/j.conb.2015.08.005
- 762 Sia GM, Clem RL, Hugarir RL. 2013. The human language-associated gene SRPX2 regulates
763 synapse formation and vocalization in mice. *Science (80-)* **342**:987–991.
764 doi:10.1126/science.1245079
- 765 Sigoillot SM, Iyer K, Binda F, González-Calvo I, Talleur M, Vodjdani G, Isope P, Selimi F.
766 2015. The Secreted Protein C1QL1 and Its Receptor BAI3 Control the Synaptic
767 Connectivity of Excitatory Inputs Converging on Cerebellar Purkinje Cells. *Cell Rep* **820–**
768 **832**. doi:10.1016/j.celrep.2015.01.034
- 769 Sotelo C. 2004. Cellular and genetic regulation of the development of the cerebellar system.
770 *Prog Neurobiol* **72**:295–339. doi:10.1016/j.pneurobio.2004.03.004
- 771 Stevens B, Allen NJ, Vazquez LE, Howell GR, Christopherson KS, Nouri N, Micheva KD,
772 Mehalow AK, Huberman AD, Stafford B, Sher A, Litke AM, Lambris JD, Smith SJ, John

- 773 SWM, Barres BA. 2007. The Classical Complement Cascade Mediates CNS Synapse
774 Elimination. *Cell* **131**:1164–1178. doi:10.1016/j.cell.2007.10.036
- 775 Stoodley CJ. 2016. The Cerebellum and Neurodevelopmental Disorders. *The Cerebellum* **15**:34–
776 37. doi:10.1007/s12311-015-0715-3
- 777 Stoodley CJ, D’Mello AM, Ellegood J, Jakkamsetti V, Liu P, Nebel MB, Gibson JM, Kelly E,
778 Meng F, Cano CA, Pascual JM, Mostofsky SH, Lerch JP, Tsai PT. 2018. Author
779 Correction: Altered cerebellar connectivity in autism and cerebellar-mediated rescue of
780 autism-related behaviors in mice (Nature Neuroscience DOI: 10.1038/s41593-017-0004-1).
781 *Nat Neurosci* **21**:1016. doi:10.1038/s41593-018-0096-2
- 782 Südhof TC. 2018. Towards an Understanding of Synapse Formation. *Neuron*.
783 doi:10.1016/j.neuron.2018.09.040
- 784 Suvrathan A, Payne HL, Raymond JL. 2016. Timing Rules for Synaptic Plasticity Matched to
785 Behavioral Function. *Neuron* **92**:959–967. doi:10.1016/j.neuron.2017.12.019
- 786 Tai H, Schuman EM. 2008. Ubiquitin , the proteasome and protein degradation in neuronal
787 function and dysfunction. *Nat Rev Neurosci* **9**. doi:10.1038/nrn2499
- 788 Tsai PT, Hull C, Chu Y, Greene-Colozzi E, Sadowski AR, Leech JM, Steinberg J, Crawley JN,
789 Regehr WG, Sahin M. 2012. Autistic-like behaviour and cerebellar dysfunction in Purkinje
790 cell Tsc1 mutant mice. *Nature* **488**:647–51. doi:10.1038/nature11310
- 791 Uemura T, Lee S-J, Yasumura M, Takeuchi T, Yoshida T, Ra M, Taguchi R, Sakimura K,
792 Mishina M. 2010. Trans-Synaptic Interaction of GluR δ 2 and Neurexin through Cbln1
793 Mediates Synapse Formation in the Cerebellum. *Cell* **141**:1068–1079.
794 doi:10.1016/j.cell.2010.04.035
- 795 Valera AM, Doussau F, Poulain B, Barbour B, Isope P. 2012. Adaptation of Granule Cell to
796 Purkinje Cell Synapses to High-Frequency Transmission. *J Neurosci* **32**:3267–3280.
797 doi:10.1523/JNEUROSCI.3175-11.2012
- 798 Wang SSH, Kloth AD, Badura A. 2014. The Cerebellum, Sensitive Periods, and Autism. *Neuron*
799 **83**:518–532. doi:10.1016/j.neuron.2014.07.016
- 800 Weber J, Polo S, Maspero E. 2019. HECT E3 ligases: A tale with multiple facets. *Front Physiol*
801 **10**:1–8. doi:10.3389/fphys.2019.00370
- 802 Widagdo J, Chai YJ, Ridder MC, Chau YQ, Johnson RC, Sah P, Haganir RL, Anggono V. 2015.
803 Activity-Dependent ubiquitination of GluA1 and GluA2 regulates AMPA receptor
804 intracellular sorting and degradation. *Cell Rep* **10**:783–795.
805 doi:10.1016/j.celrep.2015.01.015
- 806 Widagdo J, Guntupalli S, Jang SE, Anggono V. 2017. Regulation of AMPA Receptor
807 Trafficking by Protein Ubiquitination. *Front Mol Neurosci* **10**:1–10.
808 doi:10.3389/fnmol.2017.00347
- 809 Xia J, Chung HJ, Wihler C, Haganir RL, Linden DJ. 2000. Cerebellar long-term depression
810 requires PKC-regulated interactions between GluR2/3 and PDZ domain-containing
811 proteins. *Neuron* **28**:499–510. doi:10.1016/S0896-6273(00)00128-8
- 812 Yuzaki M. 2011. Cbln1 and its family proteins in synapse formation and maintenance. *Curr*

- 813 *Opin Neurobiol* **21**:215–220. doi:10.1016/j.conb.2011.01.010
- 814 Zhao HM, Wenthold RJ, Petralia RS. 1998. Glutamate receptor targeting to synaptic populations
815 on Purkinje cells is developmentally regulated. *J Neurosci* **18**:5517–5528.
816 doi:10.1046/j.1471-4159.1997.68031041.x
- 817 Zhu H, Meissner LE, Byrnes C, Tuymetova G, Tiffit CJ, Proia RL. 2020. The Complement
818 Regulator *Susd4* Influences Nervous-System Function and Neuronal Morphology in Mice.
819 *iScience* **23**:100957. doi:10.1016/j.isci.2020.100957
- 820 Zuo J, De Jager PL, Takahashi KA, Jiang W, Linden DJ, Heintz N. 1997. Neurodegeneration in
821 Lurcher mice caused by mutation in delta2 glutamate receptor gene [see comments]. *Nature*
822 **388**:769–773.
- 823

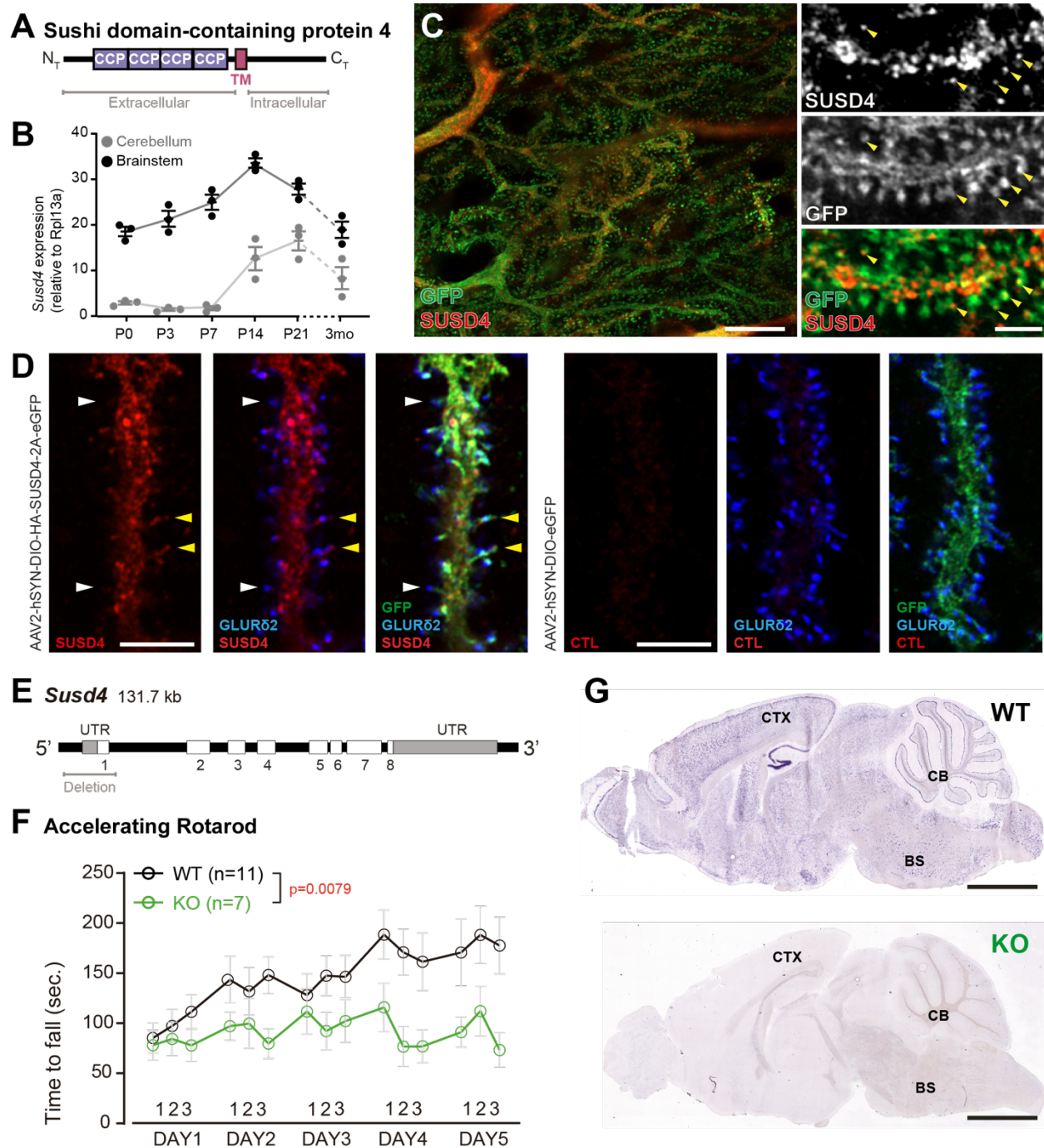


Figure 1. SUSD4 is necessary for motor coordination adaptation and learning.

- (A) Diagram of the protein SUSD4 showing its domain organization with four extracellular Complement Control Protein (CCP) domains, one transmembrane (TM) domain and a cytoplasmic domain (C_T).
- (B) Quantitative RT-PCR shows an increase in *Susd4* mRNA expression (relative to the housekeeping gene *Rpl13a*) during postnatal development in the cerebellum and in the

brainstem. Extracts were prepared from tissue samples of mice aged from 0 to 21 days (P0-21) and three months (3mo). Mean \pm s.e.m. (n=3 independent experiments).

- (C) HA-tagged SUSD4 is found in dendrites (left panel, single plane) and in some of the distal dendritic spines (right panel, arrowheads, projection of a $1,95\mu\text{m}$ z-stack) in adult cerebellar Purkinje cells. Anti-HA and anti-GFP immunolabeling was performed on parasagittal cerebellar sections obtained from adult L7-Cre mice after stereotaxic injection of AAV particles driving the expression of HA-SUSD4 and soluble GFP. Scale bars: $10\mu\text{m}$ (left panel) and $2\mu\text{m}$ (right panel).
- (D) Purkinje cells from primary mixed cerebellar culture of L7-Cre mice were transduced at 3 days in vitro (DIV3) with a HA-tagged SUSD4 expressing virus (AAV2-hSYN-DIO-HA-SUSD4-2A-eGFP) or with a control virus expressing GFP (AAV2-hSYN-DIO-eGFP), and immunostained in non-permeabilizing conditions at DIV17 for HA to localize surface SUSD4 (anti-HA, red), and in permeabilizing conditions to detect the green fluorescent protein (anti-GFP, green) and the endogenous GluD2 subunit (anti-GRID2, blue). Scale bar: $5\mu\text{m}$.
- (E) Genomic structure of the *Susd4* gene. White boxes represent exons. Exon 1 is deleted in the *Susd4* loss-of-function mouse model. See also **Figure S2**.
- (F) Motor coordination and learning is deficient in adult male *Susd4*^{-/-} (KO) mice compared to age-matched *Susd4*^{+/+} (WT) littermates. Each mouse was tested three times per day during five consecutive days on an accelerating rotarod (4 to 40 r.p.m. in 10 minutes) and the time spent on the rotarod was measured. Mean \pm s.e.m. (WT n=11 and KO n=7 mice, two-way ANOVA with repeated measures, Interaction (time and genotype): ** P=0.0079, F(14, 224) = 2.22; Time: **** P<0.0001, F(14, 224) = 3.469; Genotype: P=0.0553, F(1, 16) = 4.272).
- (G) *In situ* hybridization experiments were performed on brain sections from one month-old WT and *Susd4* KO mice to detect *Susd4* mRNA using a probe encompassing exons 2 to 5 (See also **Figure S2**). *Susd4* expression was found in many regions of the brain in *Susd4*^{+/+} (WT) mice (see also **Figure S1**) including the cerebral cortex (CTX), the cerebellum (CB), and the brainstem (BS). No labeling was found in the brain of *Susd4*^{-/-} (KO) mice. Scale bars: $500\mu\text{m}$.

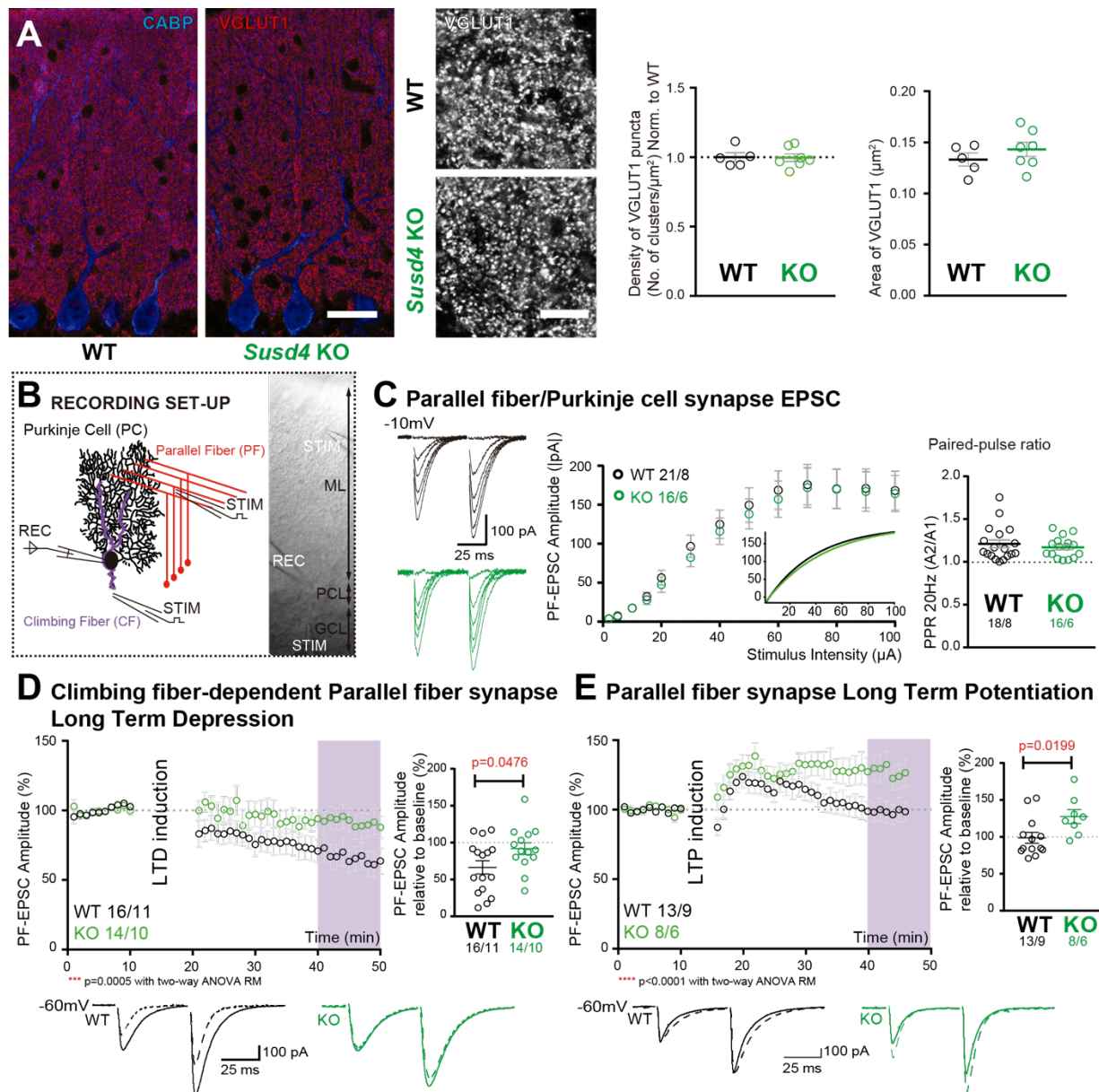


Figure 2. *Susd4* loss-of-function leads to deficient long-term depression and facilitated long-term potentiation of parallel fiber/Purkinje cell synapses.

- (A) Quantitative analysis of the morphology of parallel fiber presynaptic boutons immunolabeled by an anti-VGLUT1 antibody (red) in Purkinje cells (anti-CABP, blue). Quantifications of the density and the area of the VGLUT1 clusters did not reveal any difference between *Susd4* KO and *Susd4* WT mice. Mean \pm s.e.m. (WT n=5 and KO n=7 mice; VGLUT1 clusters density: Mann-Whitney test, $P>0.9999$; area VGLUT1 clusters: Unpaired Student t-test, $P=0.3089$). Scale bars: 30 μm (left) and 10 μm (right).
- (B) Diagram of the setup for patch-clamp recordings (REC) of Purkinje cells in 300 μm -thick parasagittal cerebellar slices. Parallel fiber and climbing fiber responses were elicited by electrical stimulation (STIM). ML: molecular layer; PCL: Purkinje cell layer; GCL: granule cell layer.

- (C) Input-output curve of the parallel fiber/Purkinje cell transmission. The amplitude of the elicited EPSCs increases with the intensity of the stimulus and is not significantly different between *Susd4* KO and WT littermates. The fitted curves for each genotype are presented in the inset. Representative sample traces are presented. Mean \pm s.e.m. (WT n=18 cells from 8 mice and KO n=16 cells from 6 mice; Kolmogorov-Smirnov test, $P=0.8793$). Short-term plasticity of parallel fiber/Purkinje cell synapses is not affected by *Susd4* loss-of-function. Parallel fibers were stimulated twice at 50 ms interval and the paired-pulse ratio (PPR) was calculated by dividing the amplitude of the second peak by the amplitude of the first peak. Mean \pm s.e.m. (WT n=21 cells from 8 mice and KO n=16 cells from 6 mice; Mann-Whitney test, $P=0.9052$).
- (D) Climbing fiber-dependent parallel fiber/Purkinje cell synapse long-term depression (LTD) is impaired in the absence of *Susd4* expression. LTD was induced by pairing stimulations of parallel fibers and climbing fibers at 100 milliseconds interval during 10 minutes at 0.5 Hz (see also **Figure S6**). The amplitude of the PF EPSC was measured using two consecutive PF stimulation at 50 milliseconds interval. Representative sample traces are presented. Right: EPSC amplitudes from the last 10 minutes (purple) of recordings were used to calculate the LTD ratio relative to baseline. Mean \pm s.e.m. (WT n=16 cells from 11 mice and KO n=14 cells from 10 mice; Two-tailed Wilcoxon Signed Rank Test with null hypothesis of 100: WT ** $p=0.0063$; KO $p=0.2676$; Mann-Whitney test, WT vs KO * $p=0.0476$).
- (E) Loss-of-function of *Susd4* facilitates parallel fiber/Purkinje cell synapse long-term potentiation (LTP). Tetanic stimulation of only parallel fibers at 0.3 Hz for 100 times (see also **Figure S6**) induced LTP in *Susd4* KO Purkinje cells while inducing only a transient increase in parallel fiber transmission in WT Purkinje cells. Representative sample traces are presented. Right: EPSC amplitudes from the last 7 minutes (purple) were used to calculate the LTP ratio relative to baseline. Mean \pm s.e.m. (WT n=13 cells from 9 mice and KO n=8 cells from 6 mice; Two-tailed Wilcoxon Signed Rank Test with null hypothesis of 100: WT $p=0.5879$; KO * $p=0.0234$; Mann-Whitney test, WT vs KO: * $p=0.0199$).

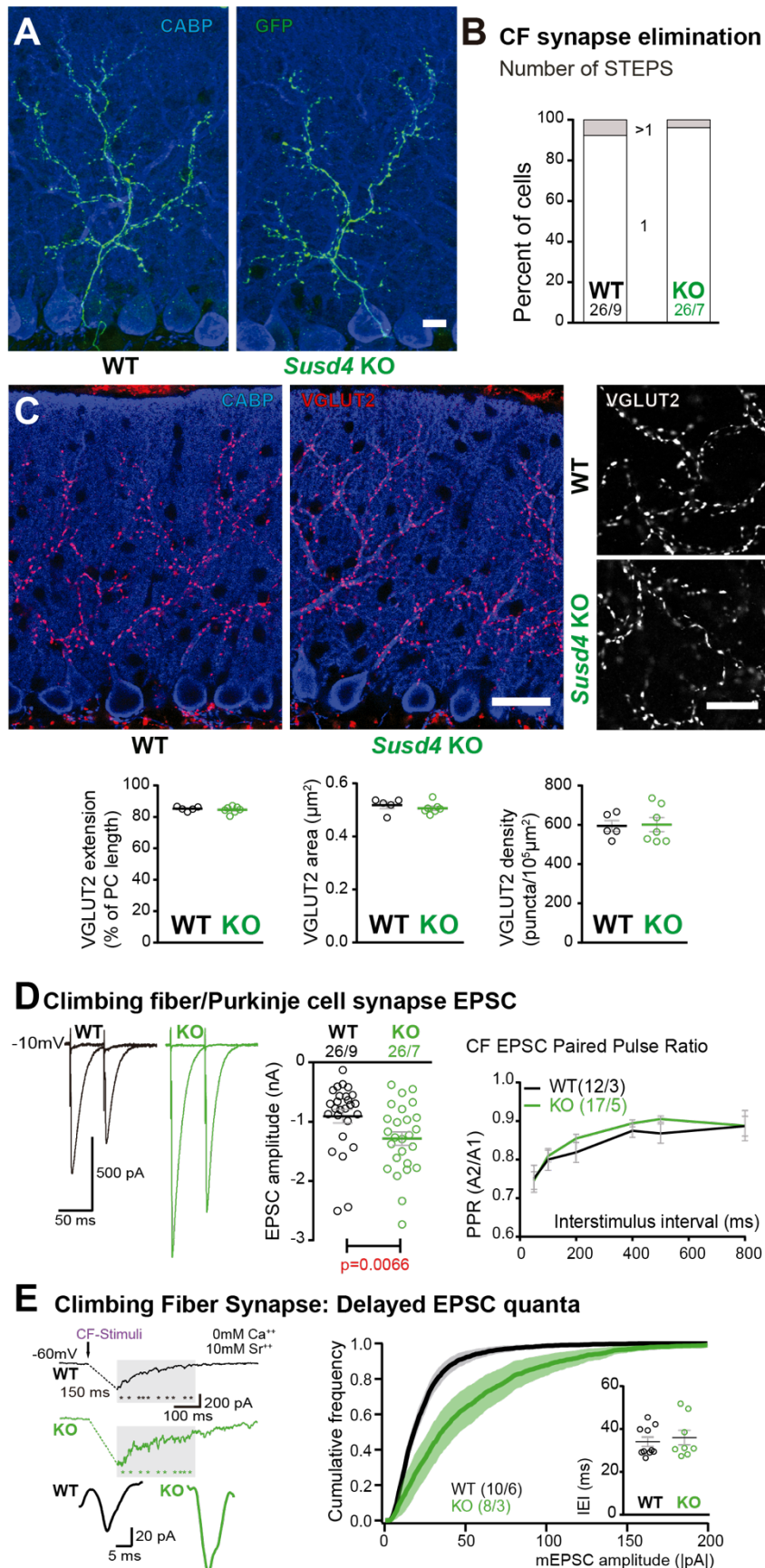


Figure 3. Transmission at the Climbing fiber/Purkinje cell synapses is increased in *Susd4* knockout mice.

(A) Left: Climbing fibers were visualized in *Susd4* WT and KO mice crossed with Htr5b-eGFP reporter mice expressing the green fluorescent protein specifically in inferior olivary neurons. Anti-GFP and anti-CABP (to visualize Purkinje cells) immunofluorescence was performed on parasagittal sections of P30 mice, and showed no qualitative differences in the absence of *Susd4* expression. Scale bar: 10 μ m.

(B) Patch-clamp recordings of Purkinje cells showed a similar percentage of mono- (1 climbing fiber) and multi-innervation (>1 climbing fibers) of Purkinje cells in P30 *Susd4* KO and WT mice, as measured by the number of steps elicited by electrical stimulation of the climbing fibers. (WT n=26 cells from 9 mice and KO n=26 cells from 7 mice; Chi-square test, P=0.5520).

(C) Climbing fiber presynaptic boutons were immunostained with an anti-VGLUT2 antibody in cerebellar sections from P30 WT and *Susd4* KO mice. The extension of the climbing fiber territory was calculated by measuring the

extent of the VGLUT2 (red) labeling relative to the height of the Purkinje cell dendritic tree (immunostained using an anti-CABP antibody, blue). Quantification of the mean density of VGLUT2 puncta and their mean area showed no differences between *Susd4* KO mice and their control littermates. Mean \pm s.e.m. (WT n=5 and KO n=7 mice; VGLUT2 extension: Mann-Whitney test, P=0.6389; VGLUT2 area: Unpaired Student t-test, p=0.4311; VGLUT2 density: Unpaired Student t-test, p=0.8925). Scale bars: 30 μ m (left) and 10 μ m (right).

- (D) Short-term synaptic plasticity of climbing fiber/Purkinje cell synapses was elicited by two consecutive stimulations at various intervals. The amplitude of the climbing fiber elicited EPSC was increased in *Susd4* KO mice compared to WT littermates. (WT n=26 cells, 9 mice and KO n=26 cells, 7 mice, Mann-Whitney test, ** P=0.0066). No difference in the paired pulse ratios (PPR) was detected at any interval between *Susd4* KO mice and WT mice. Representative sample traces are presented. See also **Figure S7**. Mean \pm s.e.m. (WT n=12 cells from 3 mice and KO n=17 cells from 5 mice; Kolmogorov-Smirnov test, P=0.4740).
- (E) Delayed CF-EPSC quanta were evoked by CF stimulation in the presence of Sr⁺⁺ instead of Ca⁺⁺ to induce desynchronization of fusion events. Representative sample traces are presented. The cumulative probability for the amplitude of the events together with the individual amplitude values for each event show an increased amplitude associated with *Susd4* loss-of-function. The individual frequency values for each cell (measured as interevent interval, IEI) present no differences between the genotypes. See also **Figure S7**. Mean \pm s.e.m. (WT n=10 cells from 6 mice and KO n=8 cells from 3 mice; Amplitude: Kolmogorov-Smirnov distribution test, *** P<0.0001; Frequency: Mann Whitney test, P=0.6334).

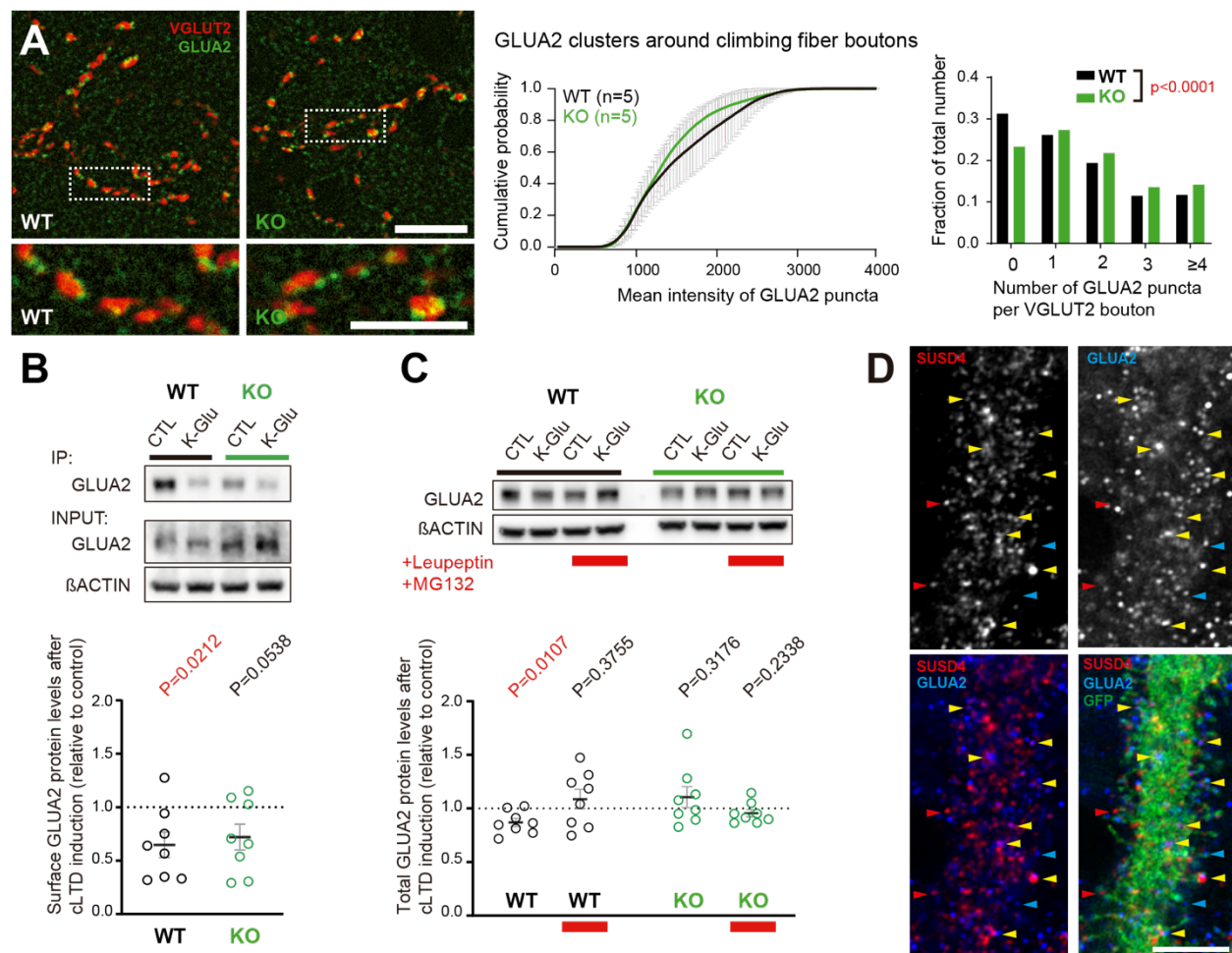


Figure 4. Loss of SUSD4 leads to misregulation of the AMPA receptor subunit GLUA2.

- (A) The number of GLUA2 clusters (anti-GLUA2 immunolabeling, green) per climbing fiber presynaptic bouton (anti-VGLUT2 immunolabeling, red) and their intensity were quantified in cerebellar sections of juvenile *Susd4*^{-/-} KO mice and *Susd4*^{+/+} WT littermates. Cumulative plot for the mean GLUA2 intensity per VGLUT2 bouton shows no significant change between WT and KO. The distribution of the VGLUT2 boutons according to the number of associated GLUA2 clusters is significantly different between WT and KO. Mean \pm s.e.m. (WT n= 5 and KO n= 5 mice; Intensity: Kolmogorov-Smirnov test, P=0.5009; Distribution: Chi-square contingency test, **** P<0.0001). Scale bars: 30 μ m (top) and 15 μ m (bottom).
- (B) Activity-dependent changes in surface localization of GLUA2 was studied in cerebellar acute slices from *Susd4* KO mice and control *Susd4* WT littermates using a chemical LTD protocol (cLTD; K-Glu: K⁺ 50mM and glutamate 10 μ M for 5 minutes followed by 30 minutes of recovery). Surface biotinylation of GLUA2 subunits was performed followed by affinity-purification of biotinylated GLUA2 subunits and anti-GLUA2 immunoblot analysis. The fraction of biotinylated GLUA2 was obtained by measuring the levels of biotinylated GLUA2 in affinity-purified samples and total GLUA2 normalized to beta-

actin in input samples for each condition. The ratios between the fraction of biotinylated GLUA2 after cLTD and control conditions are represented. Mean \pm s.e.m. (n=8 independent experiments; Two-tailed Student's one sample t-test was performed on the ratios with a null hypothesis of 1, $P_{WT} = 0.0212$ and $P_{KO} = 0.0538$).

- (C) Activity-dependent degradation of GLUA2 was assessed in cerebellar acute slices from *Susd4* KO and control mice after induction of chemical LTD (cLTD; K-Glu: K^+ 50mM and glutamate 10 μ M for 5 minutes followed by 30 minutes of recovery). This degradation was absent when slices were incubated with 100 μ g/mL leupeptin and with 50 μ M MG132 (to inhibit lysosomal and proteasome degradation, respectively), or when slices were obtained from *Susd4* KO mice. Band intensities of GLUA2 were normalized to β -ACTIN. The ratios between levels with cLTD induction (K-Glu) and without cLTD induction (CTL) are represented. See also **Figure S8**. Mean \pm s.e.m. (n=8 independent experiments; Two-tailed Student's one sample t-test was performed on the ratios with a null hypothesis of 1, $P_{WT} = 0.0107$, $P_{WT+Leu/MG132} = 0.3755$, $P_{KO} = 0.3176$ and $P_{KO+Leu/MG132} = 0.2338$).
- (D) Purkinje cells from primary cerebellar cultures of L7-Cre mice were transduced at 3 days in vitro (DIV3) with a virus driving expression of HA-tagged SUSD4 (AAV2-hSYN-DIO-HA-SUSD4-2A-eGFP) and immunolabeled at DIV17 in non-permeabilizing conditions to localize surface SUSD4 (anti-HA, red) and surface GLUA2 subunits (anti-GluA2, blue). Direct green fluorescent protein is shown (GFP, green). Examples of spines containing either SUSD4 alone, GLUA2 alone or both are shown using red, blue and yellow arrowheads, respectively (maximum projection of a 1.8 μ m z-stack). Scale bar: 5 μ m.

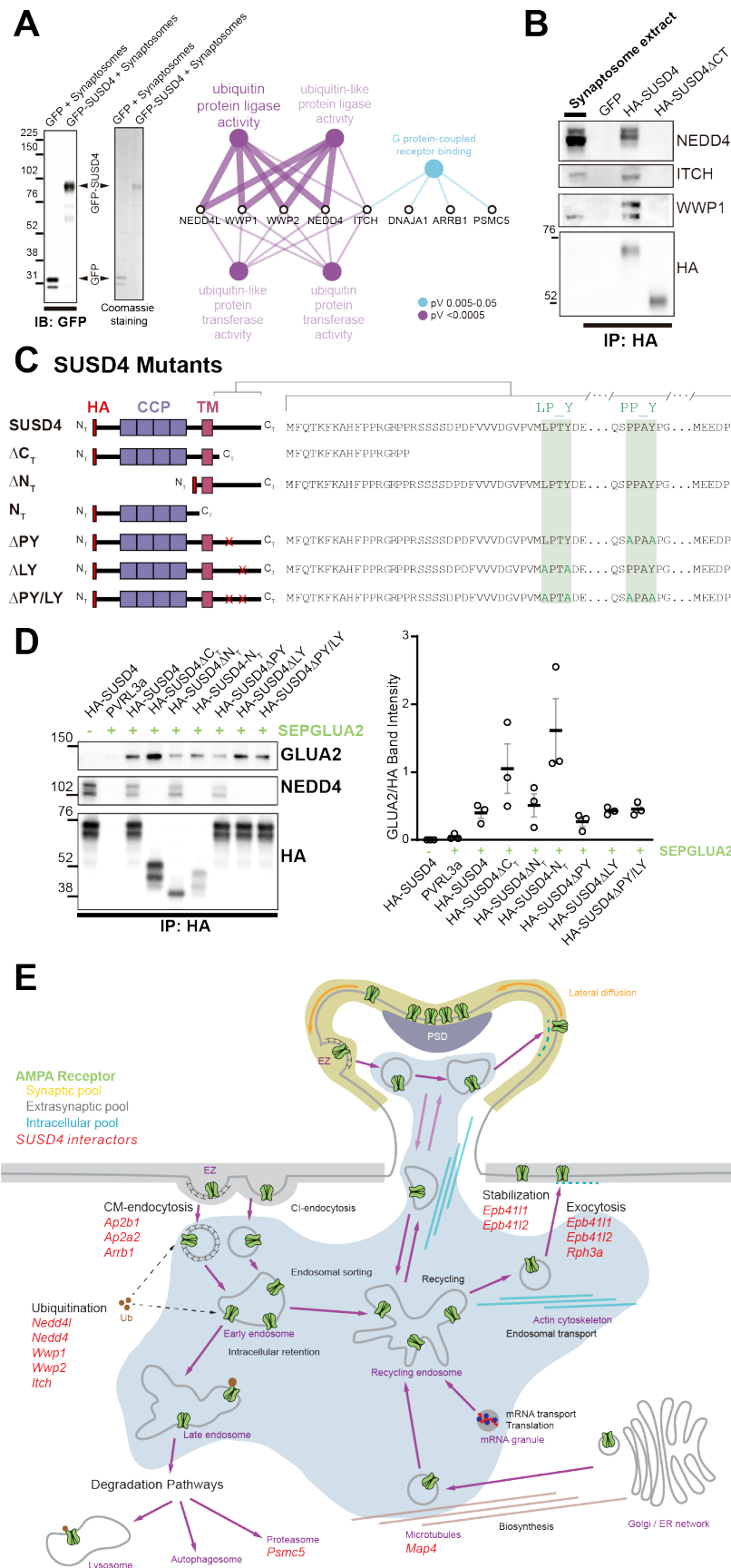


Figure 5. SUSD4 could regulate AMPA receptor degradation via multiple molecular interactions.

(A) Mass spectrometry identification of SUSD4 interactors. Left: Affinity-purification from cerebellar synaptosomes was performed using either GFP-SUSD4 as a bait or GFP as a control. Proteins were then resolved using SDS-PAGE followed by immunoblot for anti-GFP and coomassie staining of proteins. Right: Gene Ontology (GO) enrichment analysis network (Molecular Function category) of the 28 candidate proteins (Cytoscape plugin ClueGO) identified after affinity-purification of cerebellar synaptosomes using GFP-SUSD4 as a bait followed by LC MS/MS. The Ubiquitin ligase activity term is significantly enriched in particular due to the identification of several members of the NEDD4 family of HECT-ubiquitin ligase. See also **Table 1**. (n=3 independent experiments).

(B) Immunoblot confirmation of SUSD4 interaction with NEDD4 ubiquitin ligases. Affinity-purification from cerebellar synaptosomes was performed using either full length HA-SUSD4, HA-SUSD4ΔC_T or GFP as a bait. Proteins were then resolved using SDS-PAGE followed by immunoblot for NEDD4, ITCH, WWP1 or HA-SUSD4 (anti-HA). Full-length SUSD4 (HA-tagged, HA-

SUSD4) interacts with all three members of the NEDD4 family. This interaction is lost when the C-terminal tail of SUSD4 is deleted (HA-SUSD4 Δ C_T) or when GFP is used instead of SUSD4 as a control.

- (C)** Schematic representation of HA-tagged SUSD4 and different mutant constructs: SUSD4 Δ C_T (lacking the cytoplasmic tail), SUSD4 Δ N_T (lacking the extracellular domain), SUSD4N_T (lacking the transmembrane and intracellular domains), SUSD4 Δ PY (point mutation of the PPxY site), SUSD4 Δ LY (point mutation of the LPxY) and SUSD4 Δ PY/LY (double mutant at both PPxY and LPxY).
- (D)** SUSD4 interaction with GLUA2 and NEDD4 was assessed by co-immunoprecipitation using HEK293 cells transfected with SEP-GLUA2 together with PVRL3 α as a control or one of the HA-SUSD4 constructs. Affinity-purification was performed with an anti-HA antibody and extracts were probed for co-immunoprecipitation of GLUA2 (with an anti-GLUA2 antibody) and of the HECT ubiquitin ligase NEDD4 (anti-NEDD4 antibody). The level of GLUA2 co-immunoprecipitated with each SUSD4 construct was quantified by performing the ratio of GLUA2 band intensity over the HA band intensity. N=3 independent experiments.
- (E)** Potential interactors of SUSD4 control several parameters of AMPA receptor turnover. Three different pools of AMPA receptors are found in dendrites and spines: synaptic, extrasynaptic and intracellular. AMPA receptors are synthesized and delivered close to the synaptic spine to reach the synaptic surface. At the surface, AMPA receptors can move laterally (lateral diffusion) or vertically by endocytosis and exocytosis. Endocytosis can be mediated by clathrin (CM-endocytosis) or be clathrin-independent (CI-endocytosis). CM-endocytosis is often related to activity-dependent processes. After endocytosis, AMPA receptors can choose between two different pathways from the early endosomes, one for recycling and the other for degradation. Potential molecular partners of SUSD4 identified by our proteomics analysis could regulate AMPA receptor turnover at several levels of this cycle (in red).

Supplementary Information

SUSD4 controls GLUA2 degradation, synaptic plasticity and motor learning

I. González-Calvo, K. Iyer, M. Carquin, A. Khayachi, F.A. Giuliani, J. Vincent, M. Séveno, S.M. Sigoillot, M. Veleanu, S. Tahraoui, M. Albert, O. Vigy, C. Bosso-Lefèvre, Y. Nadjjar, A. Dumoulin, A. Triller, J.-L. Bessereau, L. Rondi-Reig, P. Isope, F. Selimi*

* Correspondence to: fekrije.selimi@college-de-france.fr

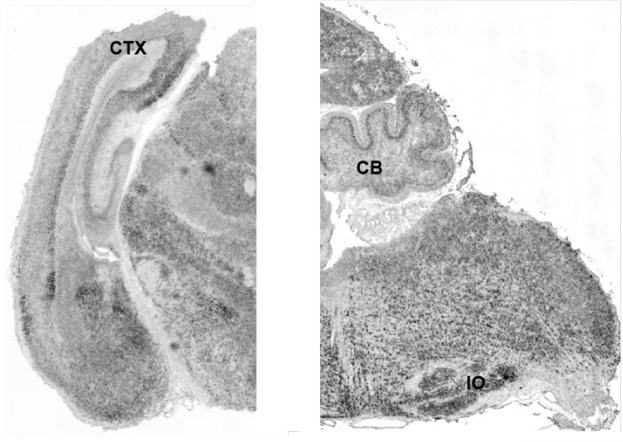
Supplementary Information:

- Table S1
- Figures S1 to S11
- Materials and Methods
- Supplementary references

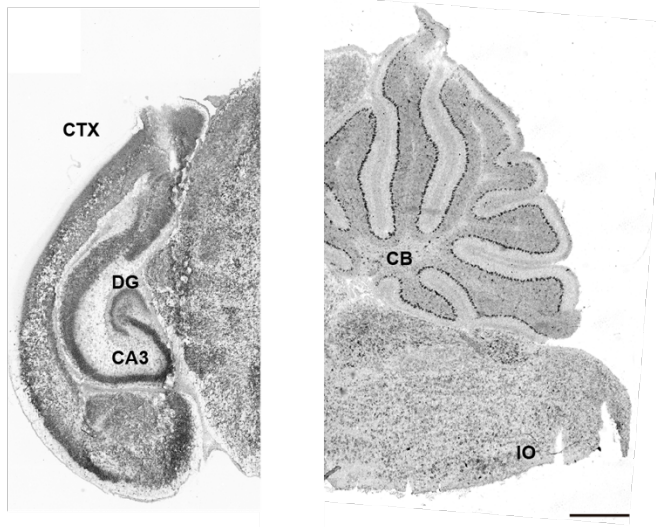
Table Supplementary 1. Behavioral characterization of *Susd4* KO mice. From three month-old *Susd4* knockout (KO) and *wild type* (WT) littermates. Mean \pm s.e.m. or percentage of mice (Physical Characteristics: WT n=10 and KO n=12 mice; Sensorimotor Reflexes and Motor responses: WT n=24 and KO n=24 mice).

	WT		<i>Susd4</i> KO	
<i>Physical Characteristics</i>				
Weight (g)	24,13	\pm 1.20	24,72	\pm 1.33
Whiskers (% with)	80	%	83,3	%
Palpebral Closure (% with)	0	%	0	%
Piloerection (% with)	20	%	25	%
<i>Sensorimotor Reflexes</i>				
<i>(% subjects displaying "normal response")</i>				
Cage movement	100	%	100	%
Whisker response	100	%	100	%
Eye Blink	100	%	100	%
Ear Twitch	100	%	100	%
<i>Motor Responses</i>				
Open Field Locomotion				
Improvement (number)	22.83	\pm 2,89	19,42	\pm 2,03
Distance (cm)	2764	\pm 235.0	2301	\pm 158,5
Speed (cm/s)	13.32	\pm 0,42	13,06	\pm 0,30
Time on Center (%)	13.30	\pm 1,33	11,18	\pm 1,26

A P0



B P7



C P30

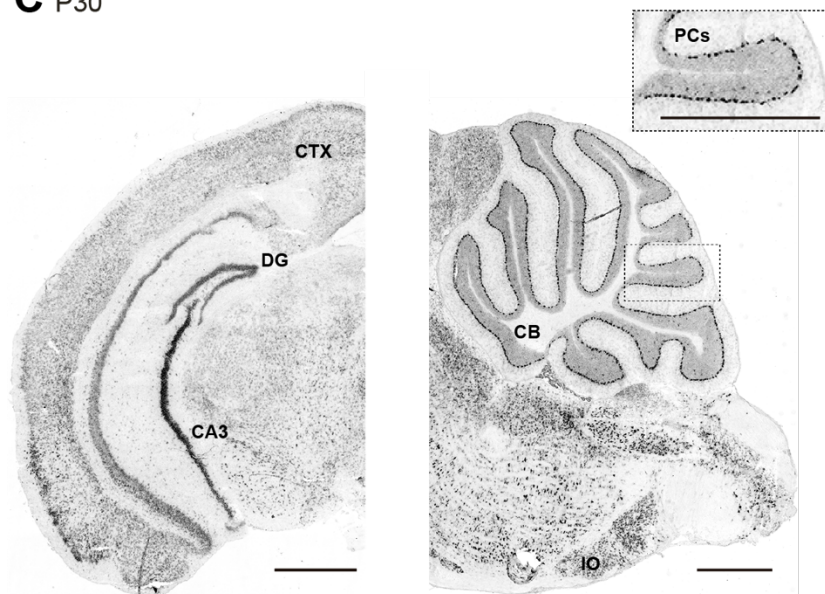


**Figure Supplementary 1.
Susd4 mRNA expression in
the developing mouse brain.**

(A) *Susd4* mRNA expression was visualized in the brain of wild-type (WT) mice by *in situ* hybridization. Coronal (left) and sagittal (right) sections are presented at postnatal day 0 (P0),

(B) postnatal day 7 (P7) and

(C) postnatal day 30 (P30). *Susd4* expression was found in many regions including the cerebral cortex (CTX), the dentate gyrus (DG) and CA3 regions in the hippocampus (coronal section, left), the cerebellum (CB), in particular Purkinje cells (PCs), and the inferior olive (IO; sagittal section, right). Scale bars: 250 μ m and 500 μ m (inset C).

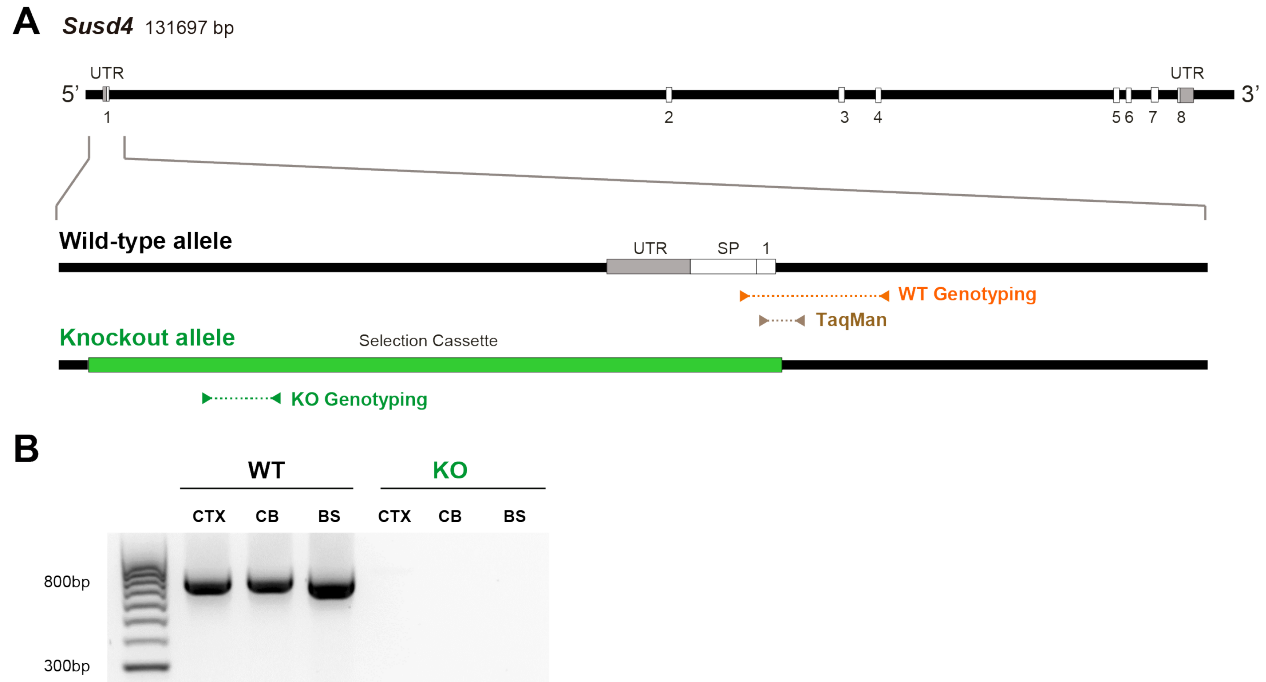


Figure Supplementary 2. Characterization of *Susd4* knockout (KO) mice.

- (A) Structure of the *Susd4* gene and strategy for the generation of the knockout mouse. The gene coding for the *Susd4* mRNA contains 8 exons. The wild-type WT allele is presented indicating the localization of the primers used for genotyping and of the probes used for TaqMan RT-qPCR. In the knockout allele, the 5'UTR and first exon are entirely deleted and replaced by the selection cassette.
- (B) *Susd4* expression was assessed by RT-PCR using primers encompassing exons 6 to 8 in extracts from cortex (CTX), cerebellum (CB) and brainstem (BS) in control and *Susd4* KO mice.

Footprint Test

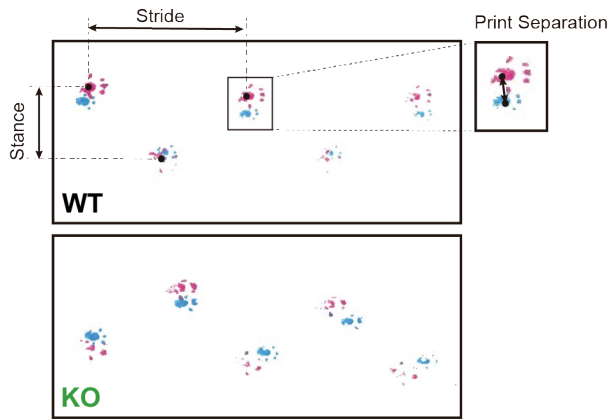
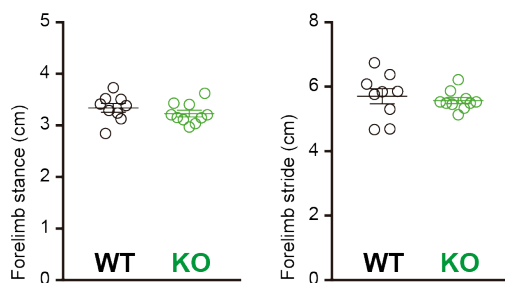


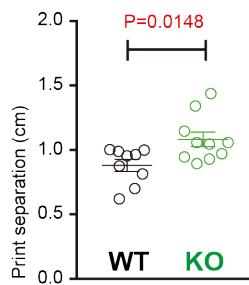
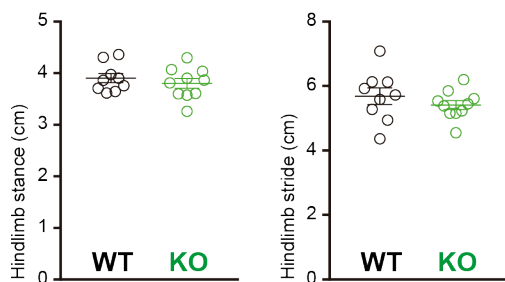
Figure Supplementary 3. Footprint analysis in *Susd4* KO mice.

Footprint patterns of P30 WT and *Susd4* KO mice were quantitatively analyzed by measuring stride length for the fore paws (magenta) and hind paws (cyan), stance length for the forelimbs and hindlimbs, and print separation. Mean \pm s.e.m. (WT n=9 and KO n=10 mice; unpaired Student's t-test; Forelimb stance: P=0.3059; Forelimb stride: P=0.5882; Hindlimb stance: P=0.4533; Hindlimb stride: P=0.3580; Print separation: * P=0.0148).

FORELIMB



HINDLIMB



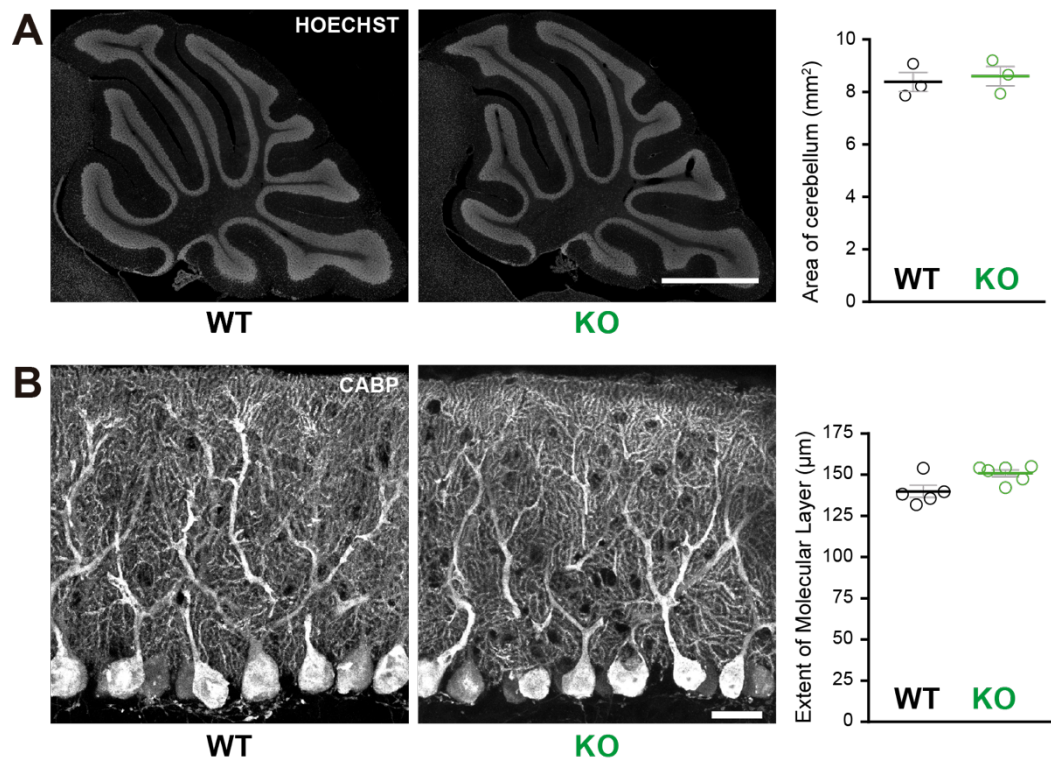


Figure Supplementary 4. Normal cerebellar cytoarchitecture in *Susd4* KO mice.

- (A) Parasagittal sections of P30 WT and *Susd4* KO cerebella were stained with Hoechst and used for quantitative analysis of the mean area of the cerebellum. Mean \pm s.e.m. (n=3 WT mice and n=3 KO mice). Scale bar: 500µm.
- (B) Calbindin protein (CABP) immunostaining was used for quantitative analysis of the mean height of the molecular layer. Mean \pm s.e.m. (WT n=5 and KO n=6 mice). Scale bar: 30µm.

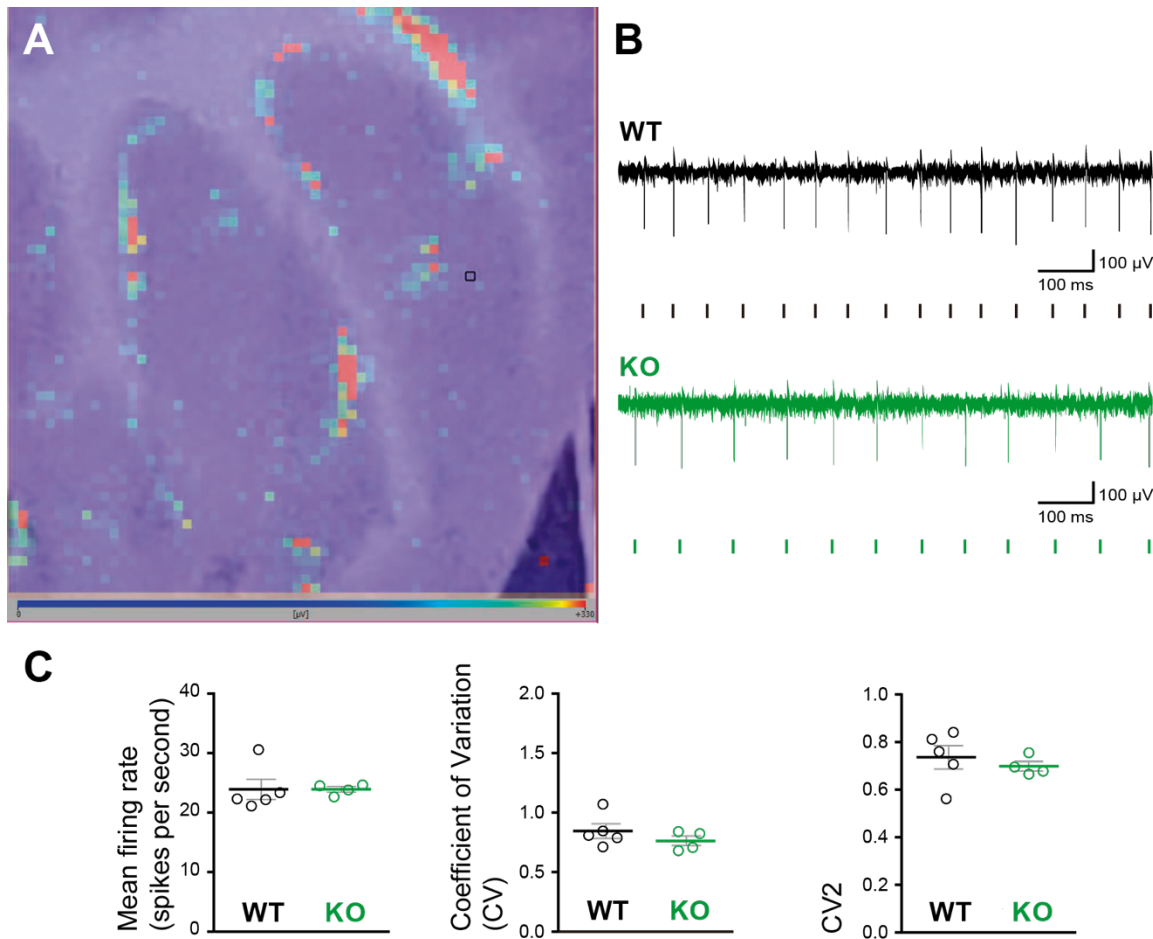


Figure Supplementary 5. High density microelectrode array (MEA) analysis of Purkinje cell spiking in acute cerebellar slices from *Susd4* KO compared to WT.

- (A) Image of a cerebellar acute slice from a WT mouse overlapped with the image of the color map of the MEA recording. Each pixel represents one channel, where the active units are in red. The black square highlights one of the channels.
- (B) Representative traces of electrical activity recorded in one channel from control and *Susd4* KO mice. Each tick points out one action potential that has been detected and sorted by the Brainwave software.
- (C) Histograms of the mean firing rate, coefficient of variation (CV) of Inter Spike Intervals and CV2. Mean \pm s.e.m. (WT n=5 and KO n=4 mice; Mann Whitney test; Mean Firing Rate: P=0.2857; CV: P=0.4127; CV2: P=0.5373).

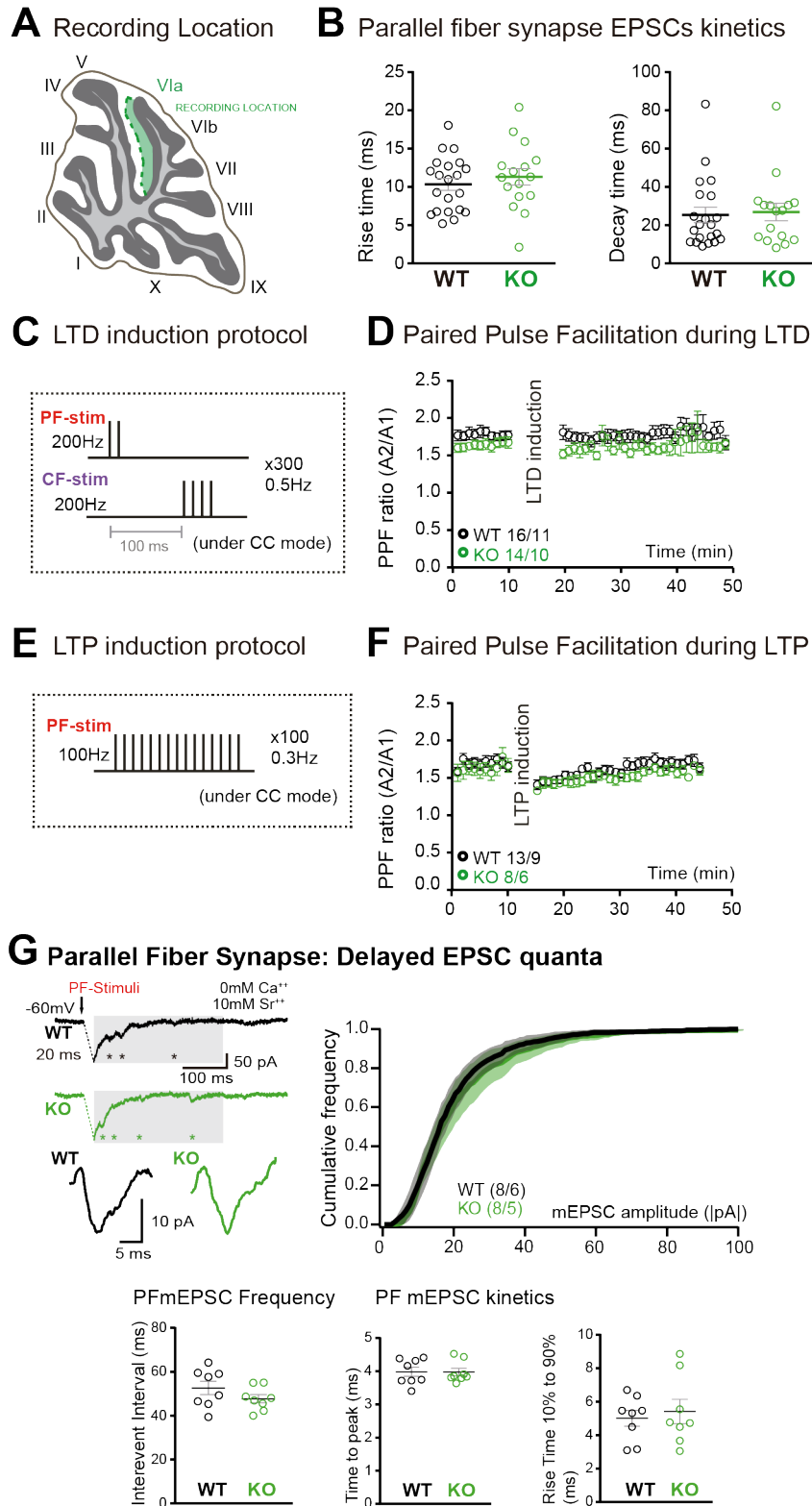
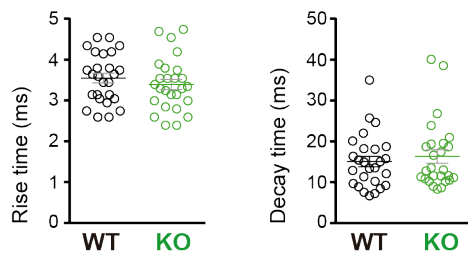


Figure Supplementary 6. Parallel fiber (PF) /Purkinje cell (PC) synapse EPSCs kinetics, long-term plasticity induction protocols, paired-pulse facilitation ratio and delayed EPSC quanta.

- (A) Schematic representation of the recording location (internal lobule VIa of the vermis).
- (B) No change in the rise time and decay of Parallel fiber/Purkinje cell EPSCs was induced by *Susd4* deletion. Mean \pm s.e.m. (WT n=21 cells from 8 mice and KO n=16 cells from 6 mice; Rise time: unpaired Student's t-test, P=0.4570; Decay time: Mann Whitney test, P=0.7276).
- (C) Parallel fiber long-term depression (LTD) induction protocol.
- (D) Paired-pulse ratio (A2/A1) during LTD measured at 20 Hz. Mean \pm s.e.m. (WT n=16 cells from 11 mice and KO n=14 cells from 10 mice; two-way ANOVA with repeated measures, Interaction (time and genotype): P=0.9935, F(39, 1092)=0.5222).
- (E) Parallel fiber long-term potentiation (LTP) induction protocol.
- (F) Paired-pulse ratio (A2/A1) during LTP measured at 20Hz. Mean \pm s.e.m. (WT n=13 cells from 9 mice and KO n=8 cells from 6 mice, two-way ANOVA with repeated measures, Interaction (time and genotype): P=0.9366, F(39, 741)=0.6745).
- (G) Delayed PF-EPSC quanta were evoked by PF stimulation in the presence of strontium (Sr⁺⁺) instead of calcium (Ca⁺⁺) to induce desynchronization of fusion events. Representative sample traces are presented. The cumulative probability for the amplitude shows no difference with *Susd4* loss-of-function. The individual frequency values for each cell (measured as interevent interval) present no differences between the genotypes. No change in the time to peak and in the rise time of PF/PC synapse delayed EPSC quanta was induced by *Susd4* deletion. Mean \pm s.e.m. (WT n=8 cells from 6 mice and KO n=8 cells from 5 mice; Amplitude: Kolmogorov-Smirnov distribution test, P=0.1667; Frequency: Mann Whitney test, P=0.1913; Time to peak: Mann Whitney test, P=0.6454; Rise time 10% to 90%: unpaired Student's t-test, P=0.6486).

A Climbing fiber synapse EPSCs kinetics



B Climbing fiber synapse mEPSCs kinetics

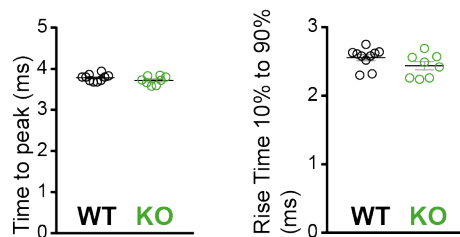


Figure Supplementary 7. Kinetics of the climbing fiber/Purkinje cell synapse EPSC.

- (A) No change in the rise and decay times of climbing fiber/Purkinje cell EPSCs was induced by *Susd4* deletion. Mean \pm s.e.m. (WT n=26 cells from 9 mice and KO n=26 cells from 7 mice; Rise time: unpaired Student's t-test, P=0.3750; Decay time: Mann Whitney test, P=0.7133).
- (B) No change in the time to peak and in the rise time of CF/PC synapse delayed EPSC quanta was induced by *Susd4* loss-of-function. Mean \pm s.e.m. (WT n=10 cells from 6 mice and KO n=8 cells from 3 mice; Time to peak: unpaired Student's t-test, P=0.1692; Rise time 10% to 90%: Mann Whitney test, P=0.0639).

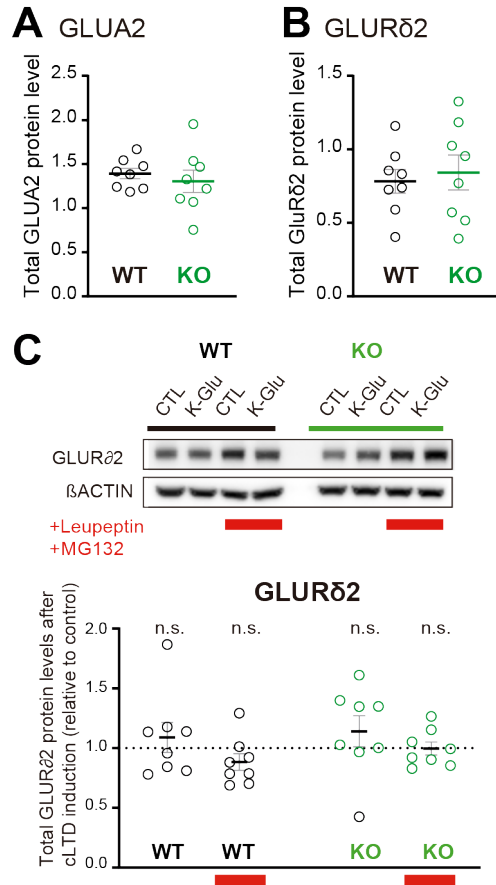


Figure Supplementary 8. Total GLUA2 and GLUR δ 2 levels after modulation of SUSD4 expression.

- (A) and (B) Total protein levels (normalized to β ACTIN) of GLUA2 (A) and GLUR δ 2 (B) were not changed in acute cerebellar slices from WT or *Susd4* KO mice in basal conditions. Mean \pm s.e.m. (n=8 independent experiments; unpaired Student's t-test; GLUA2: P=0.5424; GLUR δ 2: P=0.6821).
- (C) Cerebellar acute slices from control WT and *Susd4* KO mice were incubated to induce chemical LTD (cLTD; K-Glu: K⁺ 50mM and glutamate 10 μ M for 5min followed by 30min of recovery). Slices were incubated with 100 μ g/mL leupeptin and with 50 μ M MG132 (to inhibit lysosomal and proteasome degradation, respectively). Band intensities of GLUR δ 2 were normalized to β ACTIN. The ratios between levels with cLTD induction (K-Glu) and without cLTD induction (CTL) are represented. Mean \pm s.e.m. (n=8 independent experiments; two-tailed Student's one sample t-test was performed on the ratios with a null hypothesis of 1, P_{WT} = 0.4973, P_{WT+Leu/MG132} = 0.1433, P_{KO} = 0.3143, P_{KO+Leu/MG132} = 0.9538, n.s.= not significant).

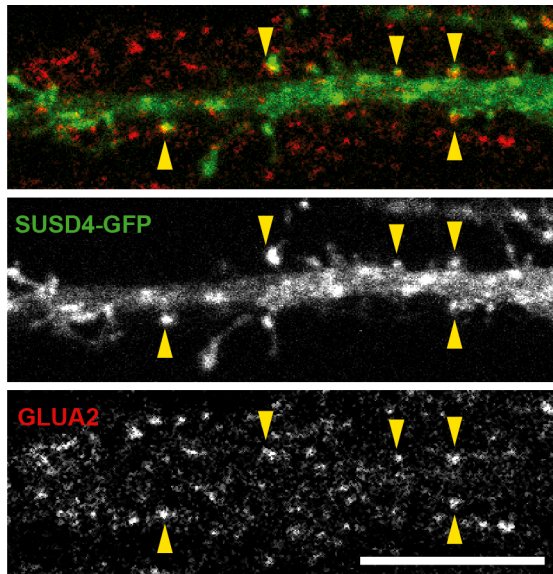


Figure Supplementary 9. HA-SUSD4 colocalizes with AMPA receptor subunit GLUA2 in hippocampal neurons.

Mouse hippocampal neurons were transfected at 13 days *in vitro* (DIV13) with a GFP-tagged SUSD4 construct and immunostained at DIV17 for green fluorescent protein (GFP, green) to localize SUSD4 and for the endogenous GLUA2 subunit (anti-GLUA2, red). The arrowheads indicate the spines containing SUSD4 and GLUA2. Scale bar: 10 μ m.

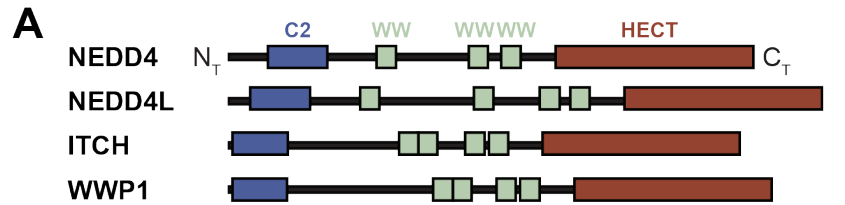
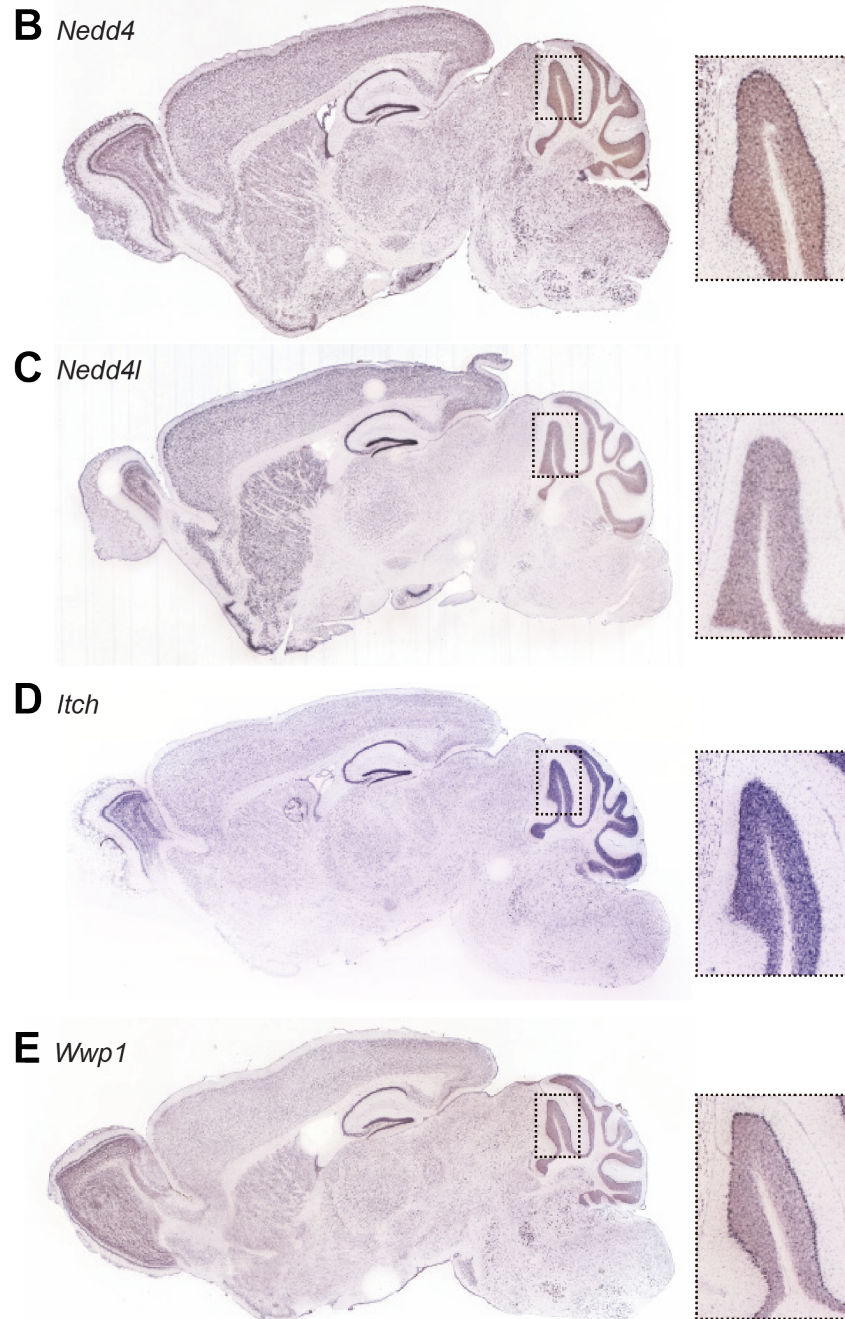


Figure Supplementary 10.
Expression of HECT ubiquitin ligases in adult mouse brain.



(A) Schematic representation of four SUSD4 interactors: NEDD4, NEDD4L, ITCH and WWP1. Legends: N_T, N-terminus; HECT, Homologous to the E6-AP C-terminus domain; C_T, C-terminus.

(B) Pattern of expression of *Nedd4* (RP_050712_03_C08),

(C) *Nedd4l* (RP_040625_01_G10),

(D) *Itch* (RP_050222_01_H06) and

(E) *Wwp1* (RP_050510_02_E12)

mRNA in the adult mouse brain. From Allen Brain Atlas (www.brain-map.org).

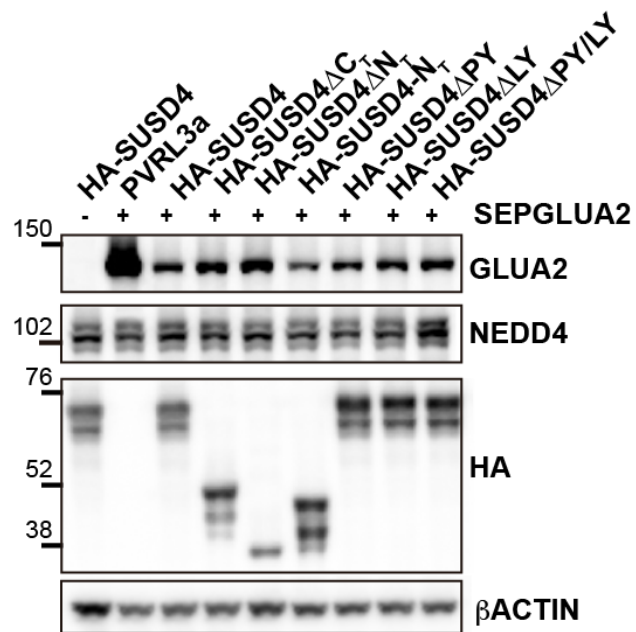


Figure Supplementary 11. Total protein levels in HEK293 cells transfected with SEP-GLUA2 and different SUSD4 mutant constructs (related to figures 5C and 5D)

HEK293 cells were transfected with SEP-GLUA2 together with PVRL3 α as a control or one of the HA-SUSD4 constructs for coimmunoprecipitation experiments. Input extracts were probed for GLUA2 (with an anti-GLUA2 antibody), the HECT ubiquitin ligase NEDD4 (anti-NEDD4 antibody), and the HA-tagged SUSD4 constructs (anti-HA antibody). β -ACTIN was used as a loading control. Representative image of N=3 independent experiments.

Materials and Methods

Animals

Susd4 knockout (KO) mice were generated and maintained on the C57BL/6J background (generated by Lexicon Genetics Incorporated, The Woodlands, USA)(Tang et al., 2010). Out of the 8 *Susd4* exons, coding exon 1 (NCBI accession NM_144796.2) and the 5'UTR (NCBI accession BM944003) were targeted by homologous recombination. This resulted in the deletion of a 1.3kb sequence spanning the transcription initiation site and exon 1 (**Figure 1E** and **Supplementary Figure 2A**). Subsequent genotyping of mice was performed using PCR to detect the wild-type (WT) allele (forward primer: 5' CTG TGG TTT CAA CTG GCG CTG TG 3'; reverse primer: 5' GCT GCC GGT GGG TGT GCG AAC CTA 3') or the targeted allele (forward primer: 5' TTG GCG GTT TCG CTA AAT AC 3'; reverse primer: 5' GGA GCT CGT TAT CGC TAT GAC 3'). Heterozygous *Susd4*^{+/-} mice were bred to obtain all the genotypes needed for the experiments (*Susd4*^{+/+} (WT) and *Susd4*^{-/-} (KO) mice) as littermates.

The *Htr5b*-GFP mouse line was used for labeling of climbing fibers (CF; The Gene Expression Nervous System Atlas (GENSAT) Project, NINDS Contracts N01NS02331 & HHSN271200723701C to The Rockefeller University (New York, NY)). Genotyping was performed using the following primers: 5' TTG GCG CGC CTC CAA CAG GAT GTT AAC AAC 3' and 5' CGC CCT CGC CGG ACA CGC TGA AC 3' (**Figure Supplementary 2A**).

The *L7Cre* mouse line was obtained from Jackson laboratories (B6.129-Tg(Pcp2-cre)2Mpin/J ; Stock Number: 004146) and genotyping was performed using the following primers: 5' GGT GAC GGT CAG TAA ATT GGA C 3'; 5' CAC TTC TGA CTT GCA CTT TCC TTG G 3' and 5' TTC TTC AAG CTG CCC AGC AGA GAG C 3'.

All animal protocols were approved by the *Comité Regional d'Ethique en Experimentation Animale* (no. 00057.01) and animals were housed in authorized facilities of the CIRB (# C75 05 12).

Antibodies

The following primary antibodies were used: mouse monoclonal anti-CABP (1:1000; Swant, Switzerland, Cat#300), rabbit polyclonal anti-CABP (1:1000; Swant, Cat#CB38), mouse monoclonal anti-GFP (1:1000; Abcam, Cambridge, United Kingdom, Cat#ab1218), rabbit polyclonal anti-GFP (1:1000; Abcam, Cat#ab6556), mouse monoclonal anti-GLUA2 (clone 6C4; 1:500; Millipore, Massachusetts, USA, Cat#MAB397 and BD, New Jersey, USA, Cat#556341), rabbit monoclonal anti-GLUA2 (1:1000; Abcam, Cat#ab206293), rabbit polyclonal anti-GLUR δ 1/2 (1:1000; Millipore, Cat#AB2285), rat monoclonal anti-HA (1:1000; Roche Life Science, Penzberg, Germany, Cat#11867423001), rabbit monoclonal anti-ITCH (1:1000; Cell Signaling Technology, Massachusetts, USA, Cat#12117), rabbit polyclonal anti-NEDD4 (1:10000; Millipore, Cat#07-049), mouse anti-ubiquitin proteins antibody (clone FK2; Enzo, New York, USA, Cat#BML-PW8810 and Sigma, Gothenburg, Sweden, Cat#04-263), guinea pig polyclonal anti-VGLUT1 (1:5000; Millipore, Cat#AB5905), guinea pig polyclonal anti-VGLUT2 (1:5000; Millipore, Cat#AB2251) and rabbit polyclonal anti-WWP1 (1:2000; Proteintech, Chicago, USA, Cat#13587-1-AP).

The following secondary antibodies were used: donkey polyclonal anti-Goat Alexa Fluor 568 (1:1000; Invitrogen, California, USA, Cat#A11057), donkey anti-Mouse Alexa Fluor 488 (1:1000; Invitrogen, Cat#R37114), donkey polyclonal anti-Mouse Alexa Fluor 568 (1:1000; Invitrogen, #A10037), donkey polyclonal anti-Rabbit Alexa Fluor 488 (1:1000; Invitrogen,

Cat#A21206), donkey polyclonal anti-Rat Alexa Fluor 594 (1:1000; Invitrogen, #A21209), donkey polyclonal anti-Rat Alexa Fluor 568 (1:1000; Abcam, Cat#175475), goat polyclonal anti-Guinea Pig Alexa Fluor 488 (1:1000; Invitrogen, Cat#A110-73), goat polyclonal anti-Guinea Pig Alexa Fluor 647 (1:1000; Invitrogen, Cat#A21450), goat polyclonal anti-Mouse HRP (1:10000; Jackson Immune Research Laboratories, Pennsylvania, USA, Cat#115-035-174), goat polyclonal anti-rat HRP (1:10000; Jackson Immune Research Laboratories, #112-035-175) and mouse polyclonal anti-rabbit HRP (1:10000; Jackson Immune Research Laboratories, #211-032-171).

The following conjugated antibodies were used: sheep polyclonal anti-digoxigenin alkaline phosphatase (1:2000 - 1:5000; Roche Life Science, Cat#11093274910), mouse monoclonal anti- β ACTIN (clone AC-15) HRP (1:25000; Abcam, Cat#ab49900), rabbit polyclonal anti-GFP Alexa Fluor 647 (1:1000; Invitrogen, Cat#A31852), mouse monoclonal anti-GluR2 (clone 6C4) Alexa Fluor 488 (1:1000; Millipore, Cat#MAB397A4) and mouse monoclonal anti-HA (clone 2-2.2.14) DyLight 650 (1:1000; Thermo Fisher Scientific, Massachusetts, USA, Cat#26183-D650).

Plasmids

Full-length *Susd4* mouse gene was cloned into the mammalian expression vector pEGFP-N1 (Addgene, Massachusetts, USA, Cat#6085-1) to express a SUSD4-GFP fusion construct under the control of the CMV promoter (pSUSD4-GFP). An N-terminal HA tag was inserted just after the signal peptide (pHA-SUSD4-GFP). pHA-SUSD4 was obtained by removal of the C-terminal GFP of pHA-SUSD4-GFP. A truncated form of *Susd4*, expressing the HA-SUSD4- Δ C_T mutant, was obtained by inserting a stop codon downstream of the sixth exon, 39bp after the transmembrane domain using PCR on the pHA-SUSD4-GFP plasmid and the following primers: forward primer 5' GCG CTA GCG ATG TAT CCT TAT GAT GTT CCT G 3'; reverse primer 5'TAG CGG CCG CTA TTA GGG GGG GAA GTG GGC CTT 3'. Other mutant constructs were similarly obtained: the truncated form HA-SUSD4- Δ N_T corresponding to aminoacids 294-490, and the extracellular form of SUSD4, HA-SUSD4-N_T, corresponding to aminoacids 2-299. The HA-SUSD4- Δ PY contains a mutation in aminoacids 411 and 414 changing PPAY to APAA while HA-SUSD4- Δ LY is mutated in aminoacids 376 and 379 changing LPTY to APTA. Mutagenesis was performed using the QuikChange Lightning Multi site directed mutagenesis kit (Agilent, Santa Clara, USA, Cat#210513) according to the manufacturer's instructions. The plasmid pIRES2-eGFP (Addgene, Cat#6029-1) was used as transfection control. The plasmid expressing SEPGLUA2 (Addgene, Cat#24001) was used to follow GLUA2. The control transmembrane protein PVRL3 α was cloned into the mammalian expression vector pCAG-mGFP (Addgene, Cat#14757) to express the protein under the pCAG promoter (pCAG-PVRL3 α). The plasmids expressing GFP-tagged RAB proteins (GFP-RAB4a, GFP-RAB5a, GFP-Rab7a and GFP-RAB11a) were kindly provided by Dr. Bruno Goud.

Viral mediated *in vivo* expression of HA-SUSD4

AAV2 particles were generated using a hSYN-DIO-HA-SUSD4-2A-eGFP-WPRE construct (Vector biolabs, Malvern, USA) and injected stereotaxically in cerebella of adult mice expressing the CRE recombinase in cerebellar Purkinje cells (PCs) using the L7Cre mice. In the absence of Cre expression, the transgene is not produced. In the presence of Cre expression, the transgene will be "FLip-EXchanged" leading to expression of the transgene specifically in PCs.

In situ hybridization

Fresh frozen 20 μ m thick-sections were prepared using a cryostat (Cryostar NX 70, Thermo Fisher Scientific, Ref.: 957000H) from brains of *Susd4* WT and KO mice at P0, P7 or P21. The probe

sequence corresponded to the nucleotide residues 287-1064bp (encompassing exons 2-5) for mouse *Susd4* (NM_144796.4) cDNA. The riboprobes were used at a final concentration of 0.05 μ g/ μ L, and hybridization was done overnight at a temperature of 72°C. The anti-digoxigenin-AP antibody (for details see antibodies section above) was used at a dilution of 1:5000. Alkaline phosphatase detection was done using BCIP/NBT colorimetric revelation (Roche Life Science, Cat#11681451001).

Behavioral Study

12-14 weeks old male mice were used in this study. They were housed in groups of 3-5 in standard conditions: 12h light/dark cycle, with *ad libitum* food and water access. Seven days before the beginning of behavioral test, mice were housed individually to limit inter-houses variability resulting from social relationships. All behavioral tests took place in the light cycle.

S.H.I.R.P.A. protocol: Mice performed a series of tests to ensure their general good health and motor performance and habituate them to being manipulated (Crawley, 2006). The test includes observation of appearance, spontaneous behavior, neurological reflexes, anxiety, motor coordination, balance rotarod and muscular strength tests and were performed within five days. Individuals presenting deficits during the S.H.I.R.P.A. protocol were not used for other behavioral tests.

Footprint analysis: The fore and hind paws of mice were dipped in magenta and cyan non-toxic paint, respectively. Mice were allowed to walk through a rectangular plastic tunnel (9cm W x 57cm L x 16cm H), whose floor was covered with a sheet of white paper. Habituation was done the day before the test. Five footsteps were considered for the analysis. Footprints were scanned and length measurements were made using ImageJ.

Rotarod: Mice were first habituated to the rotarod apparatus, three days before the acceleration test. The habituation protocol consists of 5min at 4 r.p.m. To evaluate the motor coordination, mice were placed on immobile rotarod cylinders, which ramped up from 0 to 45 rotations per minute in 10min. The timer was stopped when the mouse fell off the cylinder or did a whole turn with it. For a given session, this procedure was repeated three times per day separated by 60min. The session was repeated during five consecutive days.

Whole-cell patch-clamp on acute cerebellar slices

Responses to parallel fiber (PF) and CF stimulation were recorded in PCs of the lobule VI in acute parasagittal and horizontal (long-term potentiation (LTP) experiments) cerebellar slices from *Susd4* KO juvenile (from P25 to P35) or adult (~P60) mice. *Susd4* WT littermates were used as controls. Mice were anesthetized using isoflurane 4% and sacrificed by decapitation. The cerebellum was dissected in ice cold oxygenated (95% O₂ and 5% CO₂) Bicarbonate Buffered Solution (BBS) containing (in mM): NaCl 120, KCl 3, NaHCO₃ 26, NaH₂PO₄ 1.25, CaCl₂ 2, MgCl₂ 1 and D(+)-glucose 35. 300 μ m-thick cerebellar slices were cut with a vibratome (Microm HM650V: Thermo Scientific Microm, Massachusetts, USA or 7000smz-2 Campden Instruments Ltd., UK) in slicing solution (in mM): N-Methyl-D-Glucamine 93, KCl 2.5, NaH₂PO₄ 1.2, NaHCO₃ 30, HEPES 20, D(+)-Glucose 25, MgCl₂ 10, sodium ascorbate 5, thiourea 2, sodium pyruvate 3, N-acetyl-cystein 1, kynurenic acid 1 and CaCl₂ 0.5 (pH 7.3). Immediately after cutting, slices were allowed to briefly recover at 37°C in the oxygenated sucrose-based buffer (in mM): sucrose 230, KCl 2.5, NaHCO₃ 26, NaH₂PO₄ 1.25, D(+)-glucose 25, CaCl₂ 0.8 and MgCl₂ 8. D-APV and minocycline at a final concentration of 50 μ M and 50nM, respectively, were added to the sucrose-based buffer. Slices were allowed to fully recover in bubbled BBS with 50mM

minocycline at 37°C for at least 40min before starting the experiment, then maintained at RT for a maximum time of 8h (from slicing time). Patch clamp borosilicate glass pipettes with 3-6MΩ resistance were filled with the following internal solutions:

1. Cesium metanesulfonate solution (CsMe solution, for EPSC elicited from CF and PF), containing (in mM) CsMeSO₃ 135, NaCl 6, MgCl₂ 1, HEPES 10, MgATP 4, Na₂GTP 0.4, EGTA 1.5, QX314Cl 5, TEA 5 and biocytin 2.6 (pH 7.3).
2. CsMe S-solution (for delayed EPSC quanta events), containing (in mM): CsMeSO₃ 140, MgCl₂ 0.5, HEPES 10, MgATP 4, Na₂GTP 0.5, BAPTA 10 and neurobiotin 1% (pH 7.35).
3. Potassium Gluconate solution (K₂Glu solution, for PF long-term plasticity), containing (in mM): K Gluconate 136, KCl 10, HEPES 10, MgCl₂ 1, sucrose 16, MgATP 4 and Na₂GTP 0.4 (pH 7.35).

Stimulation electrodes with ~5 MΩ resistances were pulled from borosilicate glass pipettes and filled with BBS. Recordings were performed at room temperature on slices continuously perfused with oxygenated BBS. The experiment started at least 20min after the whole-cell configuration was established. The Digitimer DS3 (Digitimer Ltd) stimulator was used to elicit CF and PF and neuronal connectivity responses in PCs. Patch-clamp experiments were conducted in voltage clamp mode (except for the LTP and long-term depression (LTD) induction protocols that were made under current clamp mode) using a MultiClamp 700B amplifier (Molecular Devices, California, USA) and acquired using the freeware WinWCP written by John Dempster (<https://pureportal.strath.ac.uk/en/datasets/strathclyde-electrophysiology-software-winwcp-winedr>). Series resistance was compensated by 60-100% and cells were discarded if significant changes were detected. Currents were low-pass filtered at 2.2kHz and digitized at 20kHz.

CF and PF-EPSC experiments: To isolate the AMPARs current, the BBS was supplemented with (in mM) picrotoxin 0.1, D-AP5 10, CGP52432 0.001, JNJ16259685 0.002, DPCPX 0.0005 and AM251 0.001. CF and PF EPSCs were monitored at a holding potential of -10mV. During CF recordings, the stimulation electrode was placed in the granule cell layer below the clamped cell; CF-mediated responses were identified by the typical all-or-none response and strong depression displayed by the second response elicited during paired pulse stimulations (20Hz). The number of CFs innervating the recorded PC was estimated from the number of discrete CF-EPSC steps. PF stimulation was achieved by placing the stimulation electrode in the molecular layer at the minimum distance required to avoid direct stimulation of the dendritic tree of the recorded PC. The input-output curve was obtained by incrementally increasing the stimulation strength. Peak EPSC values for PF were obtained following averaging of three consecutive recordings, values for CF-EPSC correspond to the first recording. Short-term plasticity experiments were analyzed using a software written in Python by Antoine Valera (<http://synaptiqs.wixsite.com/synaptiqs>).

PF-Long-term plasticity experiments: PCs were clamped at -60mV. Each PF-induced response was monitored by a test protocol of paired stimulation pulses (20Hz) applied every 20s. A baseline was established during 10min of paired-pulse stimulation in the voltage clamp configuration. After that, an induction protocol was applied in current-clamp mode with cells held at -60mV. During LTD induction, the PFs were stimulated with two pulses at high frequency (200Hz) and, after 100ms, the CF was stimulated with four pulses at high frequency (200Hz) repeated every 2 seconds

for a period of 10min. During LTP induction, the PFs were stimulated with bursts of 15 pulses at high frequency (100 Hz) repeated every 3s for a period of 5min (Binda et al., 2016). Then, PCs were switched to the voltage clamp mode and paired stimulation pulses applied again, lasting 40min. All the data were normalized to the mean baseline. Long-term plasticity was analyzed with the software Igor Pro 6.05 (WaveMetrics INC, Oregon, USA).

PF and CF delayed EPSC quanta events were detected and analyzed using the software Clampfit 10.7 (Molecular Devices). PF- and CF-delayed EPSC quanta superposed events were discarded manually based on the waveform. A threshold of 10pA for minimal amplitude was used to select the CF events. 100 (PF) and 300 (CF) events for each neuron were studied by analyzing consecutive traces.

High density microelectrode array (MEA) analysis of Purkinje cell spiking in acute cerebellar slices

Experiments were performed on acute cerebellar slices obtained from 3-6 months-old mice in artificial cerebrospinal fluid (ACSF) containing (in mM): NaCl 125, KCl 2.5, D(+)Glucose 25, NaHCO₃ 25, NaH₂PO₄ 1.25, CaCl₂ 2, and MgCl₂ 1 and oxygenated (95% O₂ and 5% CO₂). Parasagittal slices (320µm) were cut at 30°C (Huang and Uusisaari, 2013) with a vibratome (7000smz-2, Campden Instruments Ltd.) at an advance speed of 0.03mm/s and vertical vibration set to 0.1 - 0.3µm. Slices were then transferred to a chamber filled with oxygenated ACSF at 37°C and allowed to recover for 1h before recordings.

For recording, the slices were placed over a high-density micro electrode array of 4096 electrodes (electrode size, 21 × 21µm; pitch, 42µm; 64 × 64 matrix; Biocam X, 3Brain, Wädenswil, Switzerland), and constantly perfused with oxygenated ACSF at 37°C. Extracellular activity was digitized at 17 kHz and data were analyzed with the Brainwave software (3Brain). The signal was filtered with a butterworth high-pass filter at 200 Hz, spikes were detected with a hard threshold set at -100µV, and unsupervised spike sorting was done by the software. We selected units with a firing rate between 15 and 100 spikes per second and we excluded units presenting more than 5% of refractory period violation (set to 3ms). Recordings were performed on two slices per animal, each slice containing between 20 and 200 active neurons, and results were then pooled for each animal.

To quantify the average variability in the firing rate, the coefficient of variation (CV) of the interspike interval (ISI) in seconds) was calculated as the ratio of the standard deviation (SD) of ISIs to the mean ISI of a given cell. To measure the firing pattern variability within a short period of two ISIs, CV2 was calculated [$CV2 = 2|ISI_{n+1} - ISI_n| / (ISI_{n+1} + ISI_n)$] (Holt and Douglas, 1996).

Affinity-purification of SUSD4 interactors from synaptosome preparations

HEK293H (Gibco, Massachusetts, USA, Cat#11631-017) were maintained at 37°C in a humidified incubator with 5% CO₂ in Dulbecco's Modified Eagle's Medium (DMEM; containing high glucose and glutamax, Life Technologies, Cat#31966047) supplemented with 10% fetal bovine serum (FBS, Gibco, Cat#16141-079), and 1% penicillin/streptomycin (Gibco, Cat#15140122). 10⁶ cells were plated per well in a 6-well plate and transfected 24 hours (h) after plating with the indicated plasmids (1µg plasmid DNA per well) using Lipofectamine 2000 (Invitrogen, Cat#11668-019) according to manufacturer's instructions.

48h after transfection, cells were lysed and proteins were solubilized for 1h at 4°C under gentle rotation in lysis buffer (10mM Tris-HCl pH7.5, 10mM EDTA, 150mM NaCl, 1% Triton X100

(Tx; Sigma, Cat#x100), 0.1% SDS) supplemented with a protease inhibitor cocktail (1:100; Sigma, Cat#P8340) and MG132 (100 μ M; Sigma, Cat#C2211). Lysates were sonicated for 10 seconds, further solubilized for 1h at 4°C and clarified by centrifugation at 6000 r.p.m. during 8 minutes (min). Supernatants were collected, incubated with 5 μ g of rat monoclonal anti-HA antibody (for details see antibodies), together with 60 μ L of protein G-sepharose beads (Sigma; Cat#10003D) for 3h at 4°C, to coat the beads with the HA-tagged SUSD4 proteins. When SUSD4-GFP was expressed for affinity-pulldowns, GFP-Trap was done according to the instructions of GFP-Trap®_A (Chromotek, New York, USA, Cat#ABIN509397). Coated beads were washed 3 times with 1mL lysis buffer.

To prepare synaptosome fractions, cerebella from WT mice (P30) were homogenized at 4°C in 10 volumes (w/v) of 10mM Tris buffer (pH7.4) containing 0.32M sucrose and protease inhibitor cocktail (1:100). The resulting homogenate was centrifuged at 800g for 5min at 4°C to remove nuclei and cellular debris. Synaptosomal fractions were purified by centrifugation for 20min at 20000 r.p.m. (SW41Ti rotor) at 4°C using Percoll-sucrose density gradients (2-6-10-20%; v/v). Each fraction from the 10 - 20% interface was collected and washed in 10mL of a 5mM HEPES buffer pH 7.4 (NaOH) containing 140mM NaCl, 3mM KCl, 1.2mM MgSO₄, 1.2mM CaCl₂, 1mM NaH₂PO₄, 5mM NaHCO₃ and 10mM D(+)-Glucose by centrifugation. The suspension was immediately centrifuged at 10000g at 4°C for 10min. Synaptosomes in the pellet were resuspended in 100 μ L of lysis buffer (10mM Tris-HCl pH7.5, 10mM EDTA, 150mM NaCl, 1% Tx) supplemented with a protease inhibitor cocktail (1:100) and MG132 (100 μ M). Lysates were sonicated for 10 seconds, and further incubated for 1h at 4°C. HA-SUSD4, GFP-SUSD4 or its control GFP coated beads were then incubated with the synaptosomal lysates for 3h at 4°C. Beads were washed three times with lysis buffer supplemented with 0.1% SDS. Bound proteins were eluted for 10min at 75°C using Laemmli buffer (160mM Tris pH6.8, 4% SDS, 20% glycérol, 0.008% BBP) with 5% β -mercaptoethanol before SDS-PAGE followed by western blotting or mass spectrometry.

Co-Immunoprecipitation experiments in HEK293 cells

10⁶ HEK293H cells were plated per well in 6-well plates and transfected 24h after plating with the indicated plasmids (1.6 μ g plasmid SEPGLUA2 per well, using a molar ratio of 2:1 SEPGLUA2:other plasmid) using Lipofectamine 2000 according to manufacturer's instructions. For anti-HA pull downs, proteins from HEK293 cell lysates were solubilized in lysis buffer (1M Tris-HCl pH8, 10mM EDTA, 1,5M NaCl, 1% Tergitol™ (sigma; Cat#NP40), 2% Na azide, 10% SDS and 10% Na deoxycholate) supplemented with a protease inhibitor cocktail (1:100) and MG132 (1%). Then, lysates were sonicated for 15s, further clarified by a centrifugation at 14000 r.p.m. for 10min. Supernatants were collected and incubated with Dynabeads protein G (life technologies, Cat#10004D) and 28.8 μ g of rat monoclonal anti-HA antibody (for details see antibodies) under gentle rotation for 1h at 4°C. Precipitates were washed three times in lysis buffer and then eluted by boiling (65°C) the beads 15min in sample buffer (made from sample buffer 2X concentrate, Sigma, Cat#S3401) before SDS-PAGE. For SEPGLUA2 pull downs, 48h after transfection, cells were washed twice in 1X PBS, lysed with 200 μ L of lysis buffer (50mM Tris-HCl pH8 and 1% Tx) supplemented with a protease inhibitor cocktail (1:100) and MG132 (50 μ M), scraped, sonicated 3 x 5 seconds, and proteins were further solubilized for 30min at 4°C under rotation. Lysates were clarified by centrifugation at 14000 r.p.m. for 10min at 4°C. Supernatants (inputs) were collected and incubated with G-protein Dynabeads (ThermoFisher Scientific, Cat#10004D), previously linked to mouse anti-GFP antibody (for details see antibodies section),

under gentle rotation for 1h at 4°C, to coat the beads with the SEP-tagged GLUA2 proteins and interactors. Using a magnet, coated beads were washed five times in lysis buffer and bound proteins were then eluted by boiling for 15min at 65°C in 1X sample buffer before SDS-PAGE and western blot analysis for detection of HA-SUSD4 and GLUA2.

Mass spectrometry analysis

Proteins were separated by SDS-PAGE on 10% polyacrylamide gels (Mini-PROTEAN® TGX™ Precast Gels, Bio-Rad, Hercules USA) and stained with Protein Staining Solution (Euromedex, Souffelweyersheim France). Gel lanes were cut into five pieces and destained with 50mM triethylammonium bicarbonate (TEABC) and three washes in 100% acetonitrile. Proteins were digested in-gel using trypsin (1.2µg/band, Gold, Promega, Madison USA), as previously described (Thouvenot et al., 2008). Digest products were dehydrated in a vacuum centrifuge.

Nano-flow liquid chromatography coupled to tandem mass spectrometry (NanoLC-MS/MS): Peptides, resuspended in 3µL formic acid (0.1%, buffer A), were loaded onto a 15cm reversed phase column (75mm inner diameter, Acclaim Pepmap 100® C18, Thermo Fisher Scientific) and separated with an Ultimate 3000 RSLC system (Thermo Fisher Scientific) coupled to a Q Exactive Plus (Thermo Fisher Scientific) *via* a nano-electrospray source, using a 120min gradient of 5 to 40% of buffer B (80% ACN, 0.1% formic acid) and a flow rate of 300nL/min.

MS/MS analyses were performed in a data-dependent mode. Full scans (375 - 1,500m/z) were acquired in the Orbitrap mass analyzer with a 70000 resolution at 200m/z. For the full scans, 3 x 10⁶ ions were accumulated within a maximum injection time of 60ms and detected in the Orbitrap analyzer. The twelve most intense ions with charge states ≥ 2 were sequentially isolated to a target value of 1 x 10⁵ with a maximum injection time of 45ms and fragmented by HCD (Higher-energy collisional dissociation) in the collision cell (normalized collision energy of 28%) and detected in the Orbitrap analyzer at 17500 resolution.

MS/MS data analysis: Raw spectra were processed using the MaxQuant environment ((Cox and Mann, 2008), v.1.5.5.1) and Andromeda for database search (Cox et al., 2011). The MS/MS spectra were matched against the UniProt Reference proteome (Proteome ID UP000000589) of *Mus musculus* (release 2017_03; <http://www.uniprot.org>) and 250 frequently observed contaminants (MaxQuant contaminants database) as well as reversed sequences of all entries. The following settings were applied for database interrogation: mass tolerance of 7ppm (MS) and 0.5 Th (MS/MS), trypsin/P enzyme specificity, up to two missed cleavages allowed, only peptides with at least seven amino acids in length considered, and Oxidation (Met) and acetylation (protein N-term) as variable modifications. The “match between runs” (MBR) feature was allowed, with a matching time window of 0.7min. FDR was set at 0.01 for peptides and proteins.

A representative protein ID in each protein group was automatically selected using an in-house bioinformatics tool (leading v2.1). First, proteins with the most numerous identified peptides are isolated in a “match group” (proteins from the “Protein IDs” column with the maximum number of “peptides counts”). For the match groups where more than one protein ID is present after filtering, the best annotated protein in UniProtKB (reviewed entries rather than automatic ones), highest evidence for protein existence, most annotated protein according to the number of Gene Ontology Annotations (GOA Mouse version 151) is defined as the “leading” protein. Only proteins

identified with a minimum of two unique peptides, without MS/MS in control immunoprecipitation and exhibiting more than 4-fold enrichment (assessed by spectral count ratio) in Sushi domain-containing protein 4 (SUSD4) immunoprecipitation, vs control immunoprecipitation, in the two biological replicates, were considered as potential partners of SUSD4 (**Table 1**).

Gene Ontology analysis: The statistically enriched gene ontology (GO) categories for the 28 candidate proteins were determined by Cytoscape (v3.6) plugin ClueGO v2.5.3 (Bindea et al., 2009). The molecular function category was considered (release 18.12.2018, <https://www.ebi.ac.uk/GOA>), except evidences inferred from electronic annotations. Terms are selected by different filter criteria from the ontology source: 3-8 GO level intervals, minimum of 4 genes per GO term and 10% of associated genes/term. A two-sided hypergeometric test for enrichment analysis (Benjamini-Hochberg standard correction used for multiple testing) was applied against the whole identified protein as reference set. Other predefined settings were used. Each node representing a specific GO term is color-coded based on enrichment significance (p-value). Edge thickness represents the calculated score (κ) to determine the association strength between the terms.

Chemical LTD and GLUA2 surface biotinylation assay in cerebellar acute slices

300 μ m-thick parasagittal cerebellar slices were obtained from P31-P69 WT and *Susd4* KO mice following the same protocol described before (Patch-clamp section). Slices were incubated for 2h at 37°C in oxygenated BBS with or without proteasome (50 μ M MG132 in DMSO,) and lysosomal (100 μ g/mL leupeptine in water, Sigma, Cat#11034626001) inhibitors. Chemical LTD was induced by incubating the slices for 5min at 37°C in BBS containing 50mM K⁺ and 10 μ M glutamate (diluted in HCl), followed by a recovery period in BBS for 30min at 37°C all under oxygenation; in presence or not of inhibitors. Control slices were incubated in parallel in BBS solution containing HCl. Slices were then homogenized in lysis buffer, containing: 50mM Tris-HCl, 150mM NaCl, 0.1% SDS, 0.02% Na Azide, 0.5% Na Deoxycholate, 1% NP-40 and protease inhibitor cocktail (1:100). Homogenates were incubated 45min at 4°C, then sonicated and centrifuged at 14000 r.p.m. for 10min at 4°C. Supernatants were then heated at 65°C in 2X sample buffer (Sigma, Cat#S3401) prior to western blot analysis for detection of GLUA2 and GLUR δ 2. For GLUA2 surface biotinylation assay, cerebellar slices (obtained from mice aged between P27-P61) were treated as above. After a recovery period of 30min at 37°C in BBS, slices were incubated in a biotinylation solution (ThermoFisher Scientific, EZ-LinkTM Sulfo-NHS-SS-Biotin, Cat#A39258, 0,125mg/mL) for 30min on ice without oxygen. Slices were finally washed three times for 10min in PBS pH7.4 at 4°C and then homogenized in lysis buffer, containing: 50mM Tris-HCl pH8, 150mM NaCl, 0.1% SDS, 0.02% Na Azide, 0.5% Na Deoxycholate, 1% NP-40 and protease inhibitor cocktail (1:100). Homogenates were incubated 45min at 4°C, then sonicated and centrifuged at 14000 r.p.m. for 10min at 4°C. Supernatants (inputs) were collected and incubated with Dynabeads MyOne Streptavidin C1 (Thermo Fisher Scientific, Cat#65001) under gentle rotation overnight at 4°C. Using a magnet, beads were washed five times in lysis buffer and biotinylated proteins were then eluted by boiling for 15min at 65°C in 1X sample buffer before SDS-PAGE and western blot analysis for detection of GLUA2.

Immunocytochemistry

Labeling of primary hippocampal neurons: Hippocampi were dissected from E18 mice embryos and dissociated. 1.2×10^5 neurons were plated onto 18 mm diameter glass cover-slips precoated with $80 \mu\text{g}/\text{mL}$ poly-L-ornithine (Sigma, Cat#P3655) and maintained at 37°C in a 5% CO_2 humidified incubator in neurobasal medium (Gibco, Cat#21103049) supplemented with 2% B-27 supplement (Gibco, Cat#17504044) and 2mM Glutamax (Gibco, Cat#35050-038). Fresh culture medium (neurobasal medium supplemented with 2% B-27, 2mM L-glutamine (Gibco, Cat#A2916801) and 5% horse serum (Gibco, Cat#26050088) was added every week for maintenance of the neuronal cultures.

Hippocampal neurons at days *in vitro* 13 (DIV13) were transfected using Lipofectamine 2000 and $0.5 \mu\text{g}$ plasmid DNA per well. After transfection, neurons were maintained in the incubator for 24h, then fixed with 100% methanol for 10min at -20°C . After rinsing with PBS, non-specific binding sites were blocked using PBS containing 4% donkey serum (DS, Abcam, Cat#ab7475) and 0.2% Tx. Primary and secondary antibodies were diluted in PBS 1% DS / 0.2% Tx and incubated 1h at room temperature. Three washes in PBS 0.2% Tx were performed before and after each antibody incubation. Nuclear counterstaining was performed with Hoechst 33342 (Sigma, Cat#14533) for 15min at room temperature.

Labeling of primary cerebellar mixed cultures: Cerebellar mixed cultures were prepared from P0 tg/0 “B6.129-Tg(Pcp2-cre)2Mpin/J” (Stock Number: 004146, outbred, C57Bl/6J background) mouse cerebella and were dissected and dissociated according to previously published protocol (Tabata et al., 2000). Neurons were seeded at a density of 5×10^6 cells/mL. Mixed cerebellar cultures were transduced at DIV3 using a Cre-dependent AAV construct that express HA-tagged SUSD4 and soluble GFP ($2 \mu\text{L}$ of AAV2-hSYN-DIO-HA-SUSD4-2A-eGFP-WPRE at $4.1 \cdot 10^{12}$ GC/mL or control AAV2-hSYN-DIO-eGFP-WPRE at $5 \cdot 10^{12}$ GC/mL). At DIV17, neurons were fixed with 4% PFA in PBS1X for 30min at room temperature. After rinsing with PBS, non-specific binding sites were blocked using PBS containing 4% DS and 0.2% Tx. Primary and secondary antibodies were diluted in PBS 1% DS and 0.2% Tx and incubated one hour at room temperature. Three PBS 0.2% Tx washes were performed before and after each antibody incubation. Nuclear counterstaining was performed with Hoechst 33342 for 15min at room temperature.

Immunohistochemistry

Labeling of brain sections: $30 \mu\text{m}$ -thick parasagittal brain sections were obtained using a freezing microtome (SM2010R, Leica) and brains obtained after intracardiac perfusion with 4% PFA in PBS solution of mice sedated with $100 \text{mg}/\text{kg}$ pentobarbital sodium. Sections were then washed three times for 5min in PBS, then blocked with PBS 4% DS for 30min. The primary antibodies were diluted in PBS, 1% DS, 1% Tx. The sections were incubated in the primary antibody solution overnight at 4°C and then washed three times for 5min in PBS 1% Tx. Sections were incubated in the secondary antibody, diluted in PBS 1% DS 1% Tx solution, for 1h at room temperature. The sections were then incubated for 15min at room temperature with the nuclear marker Hoechst 33342 in PBS 0.2% Tx. Finally, the sections were washed three times for 5min in PBS 1% Tx, recovered in PBS and mounted with Prolong Gold (Thermo Fisher Scientific, Cat#P36934) between microscope slides and coverslips (Menzel-gläser, Brunswick, Germany, Cat#15165252).

RT-PCR and quantitative RT-PCR

For standard RT-PCR, total RNA was isolated from the cortex, cerebellum and brainstem of 2-month-old *Susd4* KO mice and WT control littermates, using the RNeasy mini kit (Qiagen, Venlo, Netherlands, Cat#74104). Equivalent amounts of total RNA (100 ng) were reverse-transcribed according to the protocol of SuperScript® VILO™ cDNA Synthesis kit (Life Technologies, California, USA, Cat#11754-250) as stated by manufacturer's instructions. The primers used were forward 5' TGT TAC TGC TCG TCA TCC TGG 3' and reverse 5' GAG AGT CCC CTC TGC ACT TGG 3'. PCR was performed with an annealing temperature of 61°C, for 39 cycles, using the manufacturer's instructions (*Taq* polymerase; New England Biolabs, Massachusetts, USA, Cat#M0273S). Quantitative PCR was performed using the TaqMan universal master mix II with UNG (applied biosystems, Cat# 4440038) and the following TaqMan probes: *Rpl13a* (#4331182_Mm01612986_gH) and *Susd4* (#4331182_Mm01312134_m1).

Western Blot analysis

After samples were mixed with sample buffer, proteins were resolved by electrophoresis on a 4-12% NuPAGE Bis-Tris-Gel according to Invitrogen protocols, then electrotransferred using TransBlot DS Semi-dry transfer Cell or TransBlot Turbo transfer system (Bio-Rad) to PVDF membrane (Immobilon-P transfer membrane, Millipore, Cat#IPVH00010). Membranes were blocked in PBS supplemented with Tween 0.2% (PBST) and non-fat milk 5% and incubated with primary antibodies in PBST-milk 5%. After washing three times in PBST, membranes were incubated with Horseradish Peroxidase-conjugated secondary antibodies in PBST-milk 5%. Membranes were finally washed three times and bound antibodies were revealed using Immobilon Western (Millipore, Cat#WBKLS) or Western Femto Maximum Sensitivity (Thermo Fisher Scientific, Cat#34095) or SuperSignal West Dura (Thermo Fisher Scientific, Cat#34075) or ECL Western Blotting substrate (Thermo Fisher Scientific, Cat#32209) chemiluminescent solutions and images acquired on a Fusion FX7 system (Vilber Lourmat, Île-de-France, France). Quantitation of Western blots was performed using the ImageJ software on raw images under non-saturating conditions. Band intensities of proteins of interest were obtained after manually selecting a rectangular region around the band. The signal intensity of the band of interest was then normalized to the signal intensity of the corresponding β ACTIN (used as a loading control). For quantifications of immunoprecipitation experiments, input intensities were normalized to β ACTIN, and then the intensities of immunoprecipitated protein bands were normalized to the normalized inputs.

Image acquisition and quantification

In situ hybridization images were acquired using an Axio Zoom.V16 (Zeiss, Oberkochen, Germany) microscope equipped with a digital camera (AxioCam HRm) using a 10x objective (pixel size 0.650 μ m).

Immunofluorescence image stacks were acquired using a confocal microscope (SP5, Leica), using a 63x objective (1,4NA, oil immersion, pixel size: 57nm for cell culture imaging, pixel size: 228nm for 63x; 76nm, 57nm, 45nm for higher magnifications for *in vivo* imaging). The pinhole aperture was set to 1 Airy Unit and a z-step of 200 nm was used. Laser intensity and photomultiplier tube (PMT) gain was set so as to occupy the full dynamic range of the detector. Images were acquired in 16-bit range. Immunofluorescence images and image stacks from figure 1C, 1D and 4F were acquired using a Zeiss LSM 980 Confocal with an Airyscan detector (v2.0), using a 63x objective (1,4NA, oil immersion, pixel size: 43nm, z-step of 150nm).

Deconvolution was performed for the VGLUT1 images with Huygens 4.1 software (Scientific Volume Imaging) using Maximum Likelihood Estimation algorithm from Matlab. 40 iterations were applied in classical mode, background intensity was averaged from the voxels with lowest intensity, and signal to noise ratio values were set to a value of 25.

VGLUT1 and VGLUT2 puncta were analyzed using the Matlab software and a homemade code source (Dr. Andréa Dumoulin). The number, area and intensity of puncta were quantified using the mask of each puncta generated by the Multidimensional Image analysis software (MIA) from Metamorph® (Molecular Devices). For each animal, puncta parameters were measured from four equidistant images within a 35-image stack at 160 nm interval, acquired from three different lobules (n=12).

The software ImageJ was used to measure the total area of a cerebellar section from images of staining obtained with the nuclear marker Hoechst. The extension of the molecular layer was measured using images of the anti-CABP staining. Nine parasagittal sections were analyzed per animal. The data presented correspond to the mean per animal.

Statistical analysis

Data from all experiments were imported in Prism (GraphPad Software, California, USA) for statistical analysis, except for electrophysiology data that were imported to Igor Pro 6.05 (WaveMetrics INC) for statistical analysis.

In the case of two column analyses of means, the differences between the two groups were assessed using two-tailed Student's t-test. Normality of populations were assessed using D'Agostino & Pearson, Shapiro-Wilk and Kolmogorov-Smirnov normality tests. When groups did not fit the normal distribution, the non-parametric Mann-Whitney test was used. For the rotarod behavioral test (two variables, genotype and trial), two-way repeated measures ANOVA followed by Bonferroni post hoc test was performed. The two-tailed Student's one sample t-test (when normality criterion was met) or the two-tailed Wilcoxon Signed Rank Test was used to compare ratios to a null hypothesis of 1 for biochemical experiments or 100 for long-term plasticity (Fay, 2013). Differences in cumulative probability were assessed with the Kolmogorov-Smirnov distribution test, and differences in distribution were tested using the Chi-squared test.

Supplementary references

Binda, F., Dorgans, K., Reibel, S., Sakimura, K., Kano, M., Poulain, B., and Isope, P. (2016). Inhibition promotes long-Term potentiation at cerebellar excitatory synapses. *Sci. Rep.* *6*, 1–12.

Bindea, G., Mlecnik, B., Hackl, H., Charoentong, P., Tosolini, M., Kirilovsky, A., Fridman, W., Pagès, F., Trajanoski, Z., and Galon, J. (2009). ClueGO : a Cytoscape plug-in to decipher functionally grouped gene ontology and pathway annotation networks. *25*, 1091–1093.

Cox, J., and Mann, M. (2008). MaxQuant enables high peptide identification rates, individualized p.p.b.-range mass accuracies and proteome-wide protein quantification. *Nat. Biotechnol.* *26*, 1367–1372.

Cox, J., Neuhauser, N., Michalski, A., Scheltema, R.A., Olsen, J. V., and Mann, M. (2011). Andromeda: A peptide search engine integrated into the MaxQuant environment. *J. Proteome Res.* *10*, 1794–1805.

Crawley, J.N. (2006). *What's Wrong With My Mouse?: Behavioral Phenotyping of Transgenic and Knockout Mice: Second Edition.*

Fay, D.S. (2013). *A biologist's guide to statistical thinking and analysis.* WormBook.

Holt, G.R., and Douglas, J. (1996). Comparison of Discharge Variability Visual Cortex Neurons. *J. Neurophysiol.* 75, 1806–1814.

Huang, S., and Uusisaari, M.Y. (2013). Elevated temperature during slicing enhances acute slice preparation quality. *Front. Cell. Neurosci.* 7, 1–8.

Tabata, T., Sawada, S., Araki, K., Bono, Y., Furuya, S., and Kano, M. (2000). A reliable method for culture of dissociated mouse cerebellar cells enriched for Purkinje neurons. *J. Neurosci. Methods* 104, 45–53.

Tang, T., Li, L., Tang, J., Li, Y., Lin, W.Y., Martin, F., Grant, D., Solloway, M., Parker, L., Ye, W., et al. (2010). A mouse knockout library for secreted and transmembrane proteins. *Nat. Biotechnol.* 28, 749–755.

Thouvenot, E., Urbach, S., Dantec, C., Demetere, E., Jouin, P., Touchon, J., and Marin, P. (2008). Enhanced Detection of CNS Cell Secretome in Plasma Protein-Depleted Cerebrospinal Fluid research articles. 4409–4421.